[American Journal of Science, Vol. 321, November, 2021, P. 1308–1349, DOI 10.2475/09.2021.02]

COEXISTING ARC AND MORB SIGNATURES IN THE SONAKHAN GREENSTONE BELT, INDIA: LATE NEOARCHEAN – EARLY PROTEROZOIC SUBDUCTION ROLLBACK AND BACK-ARC FORMATION

GAUTAM KUMAR DEB*,†, DILIP SAHA**, SARBANI PATRANABIS-DEB**, and AMLAN BANERJEE**

ABSTRACT. Differentiation of rock suites related to mid-ocean ridge and subduction zone in Archean greenstone belts is important in tracing back tectonic processes related to evolution of these belts. The late Neoarchean – early Paleoproterozoic Sonakhan greenstone belt (SGB) lying between Mesoarchean gneisses of the Bastar craton and the Mesoproterozoic Chattisgarh Supergroup in central India was earlier interpreted to have arc-like affinity. New data from the SGB is presented to reinterpret the Archean tectonic setting. NNW-SSE trending SGB is constituted of three domains. The Baghmara domain in the west is dominantly a mafic metavolcanic rock succession (BGMV group), with repeated cycles of massive to pillowed basalts, pillow breccia and thin chert-BIF-shale and greywacke interlayers, representing an oceanic back-arc system. The Bilari domain in the east, with mixed mafic and felsic metavolcanic rocks (BLMV group) and minor clastic metasediments, presents an ancient magmatic arc. Overlapping these, a polymictic conglomerate-sandstone (greywacke) intercalation of the Arjuni Formation occurs in the central part of steep fold-fault belt of the SGB. Basic to intermediate intrusives (SMI group) and syn- to late-tectonic granitoids occur in all three domains.

The BGMV group samples are low-K tholeiites and characterized by modern MORB like major element composition and near-flat REE patterns, reminiscent of some basalts of back-arc spreading centres, such as Parece Vela off Mariana arc. These features together with plots in Sm/Yb versus La/Sm diagram suggest derivation of their parental magmas from primitive spinel lherzolite mantle source with an N-MORB affinity that subsequently fractionated under low-pressure conditions. The BLMV and SMI samples with calc-alkaline major element composition are characterized by E-MORB type REE profiles, with enriched LREE and fractionated HREE patterns, and enrichment in trace elements more incompatible than Ti, relative to N-MORB. In addition, plots in Sm/Yb versus La/Sm diagram indicate derivation of parental magmas from partial melting of enriched garnet lherzolite mantle source at different depths, less and more deep for the BLMV and SMI groups, respectively. The BLMV magmas evolved via crystal fractionation under high water pressure conditions. The intermediate to acidic intrusives of the SGB are calc-alkaline and metaluminous, similar to I-type granites.

Although in Th/Yb versus Nb/Yb diagram all the SGB mafic rocks plot above MORB array, restriction of the BGMV samples near N-MORB – PM field and distribution of the BLMV and SMI samples along AFC curve above the MORB array confirm juxtaposition of two contrasting suites, with oceanic back-arc and arc affinities, in the SGB. The Arjuni Formation apparently represents an accretionary wedge lodged in between the Baghmara and Bilari domains. Based on geological and geochemical characteristics, we suggest influence of subduction rollback and oceanic back-arc spreading in the tectonic evolution of the Sonakhan greenstone belt, which may have been common in other late Neoarchean – early Proterozoic greenstone belts.

Key words: Back-arc, I-type granite, MORB, Neoarchean, Sonakhan greenstone belt, Subduction rollback

* Department of Geology, Presidency University, 86/1 College Street, Kolkata 700073, India
** Geological Studies Unit, Indian Statistical Institute, 203, B. T. Road, Kolkata 700108, India
† Corresponding author: gd.geol@presiuniv.ac.in

INTRODUCTION

Recent analysis and review of chemical attributes of the volcanic rocks and provenance of sedimentary rocks from different Archean–Proterozoic supracrustal belts raise an important issue: whether an individual greenstone belt represents *in situ* development of its volcano-sedimentary succession or accreted domains, formed initially at different tectonic settings (Kusky and Kidd, 1992; Blenkinsop and others, 1993; Rollinson, 2007; Wakabayashi, 2017). In the latter case, the accreted domains may be thrust slices, and thus the supracrustal belt can be compared with ophiolite suite. The similarity in the overall association of oceanic crust and deep sea sediments, between the Proterozoic–Phanerozoic ophiolites and the Archean–Proterozoic greenstone belts has been reported earlier (for example, Dilek and Furnes, 2011). However, the common association of voluminous granitoid plutons (other than plagiogranite) and greenstone belts of the Precambrian terrains led Condie (1981) to refer to them as granite-greenstone belts. Furthermore, with access to much the same geological and geochemical data, the greenstone belts have been variously interpreted as representing MORB setting (de Wit and others, 1987), a suprasubduction zone setting (Polat and Kerrich, 2000; Polat and others, 2015; Hastie and Fitton, 2019), a continental or continent-proximal setting (Kröner and Todt, 1988), a continental back-arc setting (Sotiriou and others, 2020), as accretionary orogen (Windley and others, 2021) and an oceanic plateau (Chavagnac, 2004).

On the other hand, discrimination based on geochemical clues indicates that ophiolites may originate both at mid-ocean ridge as well as suprasubduction zone, and many of the greenstone belts can be interpreted as ophiolite (Dilek and Furnes, 2011). Contrastingly, coexistence of volcanic rocks related to mid-ocean ridge (MOR) and also subduction zone (SZ) is also common in many greenstone belts (for example, O'Neil and others, 2011) as well as in ophiolites (Shervais and others, 2019). Both the MOR- and SZ-related suites may be deformed and metamorphosed, and outcrop at convergent-margin setting. However, mode of transport of these volcano-sedimentary suites to the convergent margin may be unique as by Wilson-cycle conveyor belt for greenstone belt and by transport of thrust-scrapped oceanic crust for ophiolite. Of course, distinction on the basis of mode of transport is very difficult, because complete preservation of either greenstone belt or ophiolite is almost rare. Moreover, even the rock association of the original greenstone belts may be affected by thrusts during transport to convergent margin and thus, in turn, would be indistinguishable from the thrust-induced ophiolite. In addition, subduction rollback may have significant role in ocean-continent convergent settings (Liu and others, 2018). Obviously, differentiation between MOR- and SZ-related lithologic assemblages, if associated together, is thus as important as to correlate them from the tectono-stratigraphic point of view. And it is therefore an important challenge to explain whether coexisting MOR- and SZ-related suites, with normal or fault contact in-between, represent an artifact of ridge-trench intersection under the modern-style plate tectonics (Dilek and Furnes, 2014) or superimposed tectonic settings under the influence of stagnant-lid tectonics or plume activity (Shervais, 2001; Smithies and others, 2004; Stern, 2008; Whattam and Stern, 2011). It is noteworthy that in this regard study of the associated sedimentary rocks, typical of subduction related or unrelated settings would be helpful (Saha and others, 2017, references therein). Therefore, characterization of the sedimentary rocks coupled with assessment of petrogenetic evolution of different volcanic suites is obviously important in order to decipher the tectonic evolution of a supracrustal belt as a whole.

The peninsular India is divided into two crustal provinces, namely, the Southern Indian Block and Northern Indian Block, separated by the ENE-WSW trending Central Indian Tectonic Zone (fig. 1A; Acharyya and Roy, 2000; Roy and others, 2001;

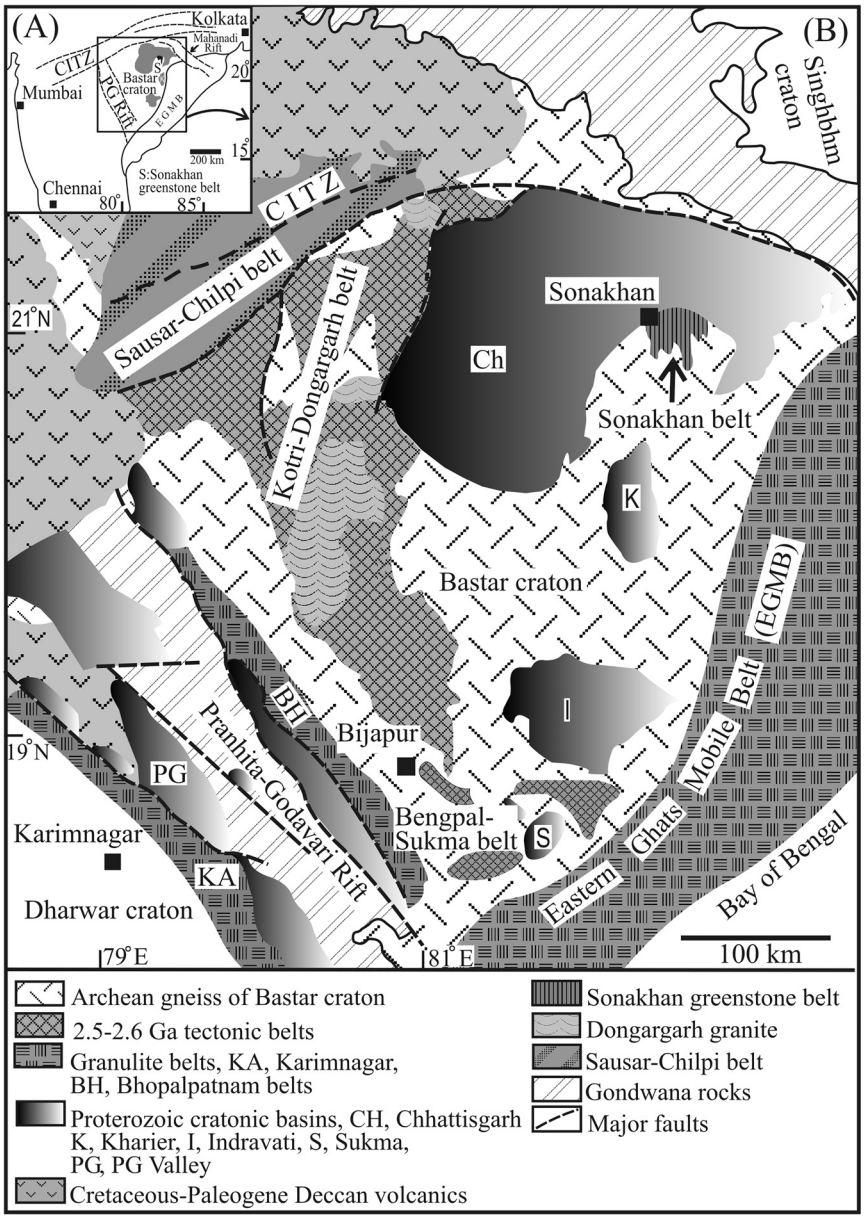

Fig. 1. Geological map of the study area, after Saha and others (2004) and Deb (2013). Inset (A) shows regional geological framework and (B) shows distribution of different tectonic and granulite belts in the Southern Indian Block, after Manu Prasanth and others (2018). CITZ, Central Indian Tectonic Zone. (C), Geological map of the Sonakhan greenstone belt showing distribution of different rock units. Lithologs along traverses across Jonk River, in the northwestern part, are presented in figure 2.

Basu and Bickford, 2015). The Bastar craton in the Southern Indian Block comprises Mesoarchean to Neoarchaean cratonic components, and is surrounded by 2.5 to 2.6 Ga supracrustal belts, including Bengpal-Sukma belt in the south, Kotri-Dogargarh belt in the west, Sausar-Chilpi belt in the north, and Sonakhan belt in the east (fig. 1B; Sarkar and others, 1990; Singh and Chabria, 2002; Manu Prasanth and others,

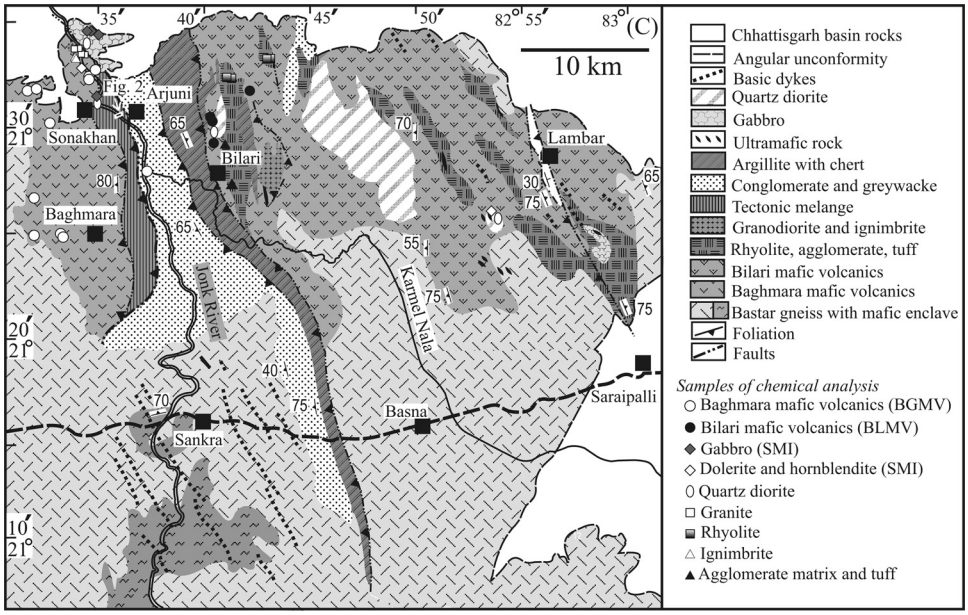

Fig. 1. (continued).

2018). The Sonakhan belt is a linear belt of greenschist facies metaigneous and metasedimentary rock assemblage, with granite intrusions, and is traditionally considered as a (granite-) greenstone belt. On the regional stratigraphic context, it was described as a Neoarchean greenstone belt (Das and others, 1990). However, the Sonakhan greenstone belt (SGB) has only been locally investigated and received much less attention compared to other greenstone belts of the peninsular Indian shield. Recently, on the basis of chemical composition of some mafic rock samples evaluation of tectonic setting of the SGB has been carried out (Mondal and Raza, 2009; Manu Prasanth and others, 2018), without providing the necessary geological and structural details for a critical assessment. Extant information on chemistry and chronology of rocks from the belt is thus insufficient for proper interpretation of its evolutionary history. In this article we present new, comprehensive results of geochemical analysis of different suites of mafic and felsic volcanic rocks, intrusive plutons of granite, diorite, gabbro and hornblendite, and their structural association with various components of the volcano-sedimentary edifice within the SGB. On the basis of these new data an attempt has been made to assess the petrogenetic evolution and tectonic context of the Sonakhan greenstone belt as a whole, and in the broader context of tectonic evolution of Archean greenstone belts, under combined influence of mantle upwelling and subduction rollback.

GEOLOGICAL SETTING

The Sonakhan greenstone belt (SGB) is NNW-SSE trending ~ 50 km wide belt, outcropped over an area of about 1000 km^2 in the northeastern part of the Bastar craton (fig. 1B). Towards north, the belt is unconformably overlain by the Chhattisgarh Supergroup (Das and others, 1990), and thus extent of this greenstone belt, further north, is still uncertain. Rocks of the SGB had earlier been classified into two groups: (i) the Sonakhan Group comprising the 'lower' metabasalt-dominated Baghmara

Formation and the 'upper' Arjuni Formation consisting mainly of polymictic conglomerate and sandstone and (ii) the Bilari Group with 'undeformed and unmetamorphosed' felsic and mafic volcanic and volcaniclastic rocks (Das and others, 1990). Later on, study by Saha and others (2004) has revealed that all the rock types of the belt were affected by polyphase deformation under greenschist facies condition. Secondly, the SGB represents a disparate association of metavolcanic and metasedimentary rocks, including (a) mafic metavolcanic rocks-dominated succession with minor chemical sediments, (b) mixed mafic and felsic metavolcanic rocks with minor clastic sediments, and (c) intrusive granite and diorite, all marked by steeply oriented foliation and showing internal deformation to various degrees. According to these authors the Sonakhan Group is divided into a lower unit dominated by metaigneous rocks with thin metasedimentary intercalation (Baghmara Formation and Bilari Group of Das and others, 1990) and an upper metasedimentary unit (Arjuni Formation of Das and others, 1990).

The SGB is flanked to the east, south and west by Archean gneiss and Proterozoic granite and granodiorite bodies of the Bastar craton (Choudhary and others, 1996; Ghosh, 2004a; Patranabis-Deb and Chaudhuri, 2008). Whole rock Rb-Sr ages on Dongargarh granite samples appear to be variable, but mostly early Paleoproterozoic, but may represent reset ages (Asthana and others, 2014; Sensarma and Mukhopadhyay, 2014). There are some preliminary reports on zircon U-Pb ages too, bracketing Dongargarh granite emplacement at 2432 ± 6 Ma (Ahmad and others, 2008). The Bijli rhyolite representing the lower part of the supracrustals (Nandgaon Group with interlayered felsic and mafic volcanic rocks, and sediments) from the Dongargarh-Kotri belt is dated 2530 Ma (U-Pb zircon; Ghosh, 2004b). The Dongargarh granite, intrusive into the Nandgaon Group supracrustals, yields a 2485 Ma U-Pb age (Bickford and others, 2014). However, on the basis of Hf isotopic compositions of zircon, indicating average single-stage T_{DM} model age of 2.99 Ga, the Dongargarh granite from the Kotri-Dongargarh belt is considered as proxy for the Bastar craton granitoid ages (Bickford and others, 2014). On the other hand, U-Pb zircon data from felsic tuffs were used to constrain 1.5 to 1.0 Ga age for the Chhattisgarh Supergroup (Patranabis-Deb and others, 2007; Bickford and others, 2011). Based on Rb-Sr age data from two samples from the eastern outcrop domain of the SGB it has been proposed by Ghosh and others (1995) that this belt might have experienced acidic volcanism twice at *ca.* 2.39 and 2.1 Ga, respectively. Both the samples, however, appear to be deformed and altered with sericitic matrix, and thus the events indicated by these Rb-Sr ages are likely reset ages. Moreover, immediately southwest of the belt, within the gneissic terrain there are NNW-SSE to NW-SE trending 1.9 to 1.8 Ga dikes of metadolerite, metapyroxinite and amphibolite (fig 1C; Srivastava and Gautam, 2008). Thus, it appears that the rocks of the belt were affected by deformation prior/close to 1.9 Ga. We, therefore, consider that the succession of the SGB possibly formed in the late Neoarchean – early Paleoproterozoic, on the Mesoarchean basement gneiss and older supracrustals of Bastar craton, and later covered by the Mesoproterozoic Chhattisgarh Supergroup.

MATERIALS AND METHODS

Field Methods

Following standard method of fieldwork, mapping of different lithounits of the SGB, their contact relations, together with systematic sampling of different domains for petrography and chemical analysis have been carried out. Furthermore, characterization of the style and sequence of mesoscopic structures has been made, in order to work out the overall structural evolution of the SGB.

TABLE 1A

Major and trace element composition of mafic lavas and intrusives of Baghmara domain

	BgM1	BgM2	BgM3	BgM4	BgM5	BgM6	BgM7	BgM8	BgM9	BgM10	BgM11	BgM12	BgM13
SiO_2	51.19	46.24	50.76	53.18	49.82	50.59	51.64	50.46	46.37	48.98	48.26	47.24	50.29
Al_2O_3	16.97	14.98	12.81	14.67	14.94	13.77	14.6	15.65	14.93	16.01	15.13	14.89	12.96
TiO_2	0.972	1.312	0.817	0.915	1.003	0.973	1.103	1.013	1.118	1.117	1.166	1.035	1.534
FeO	8.1	9.4	4.6	6.3	10.2	10.2	9.4	9.6	10.7	10.1	10.1	7	12.6
Fe_2O_3	0.73	0.69	1.31	0.87	1.05	1.65	1.28	1.17	1.56	2.45	2.44	1.35	1.81
MgO	4.29	3.84	4.09	4.78	5.97	7.34	6.55	5.62	7.09	5.12	5.09	5.52	5.48
MnO	0.166	0.217	0.158	0.134	0.195	0.171	0.189	0.2	0.198	0.183	0.183	0.108	0.225
CaO	14.04	7.67	9.86	6.72	12.93	10.45	10.48	11.49	13.43	10.83	10.6	8.71	9.46
Na_2O	1.17	3.38	3.13	3.11	1.92	2.23	2.32	2.59	1.78	2.45	2.38	3.47	2.15
K_2O	0.32	0.26	0.48	0.39	0.22	0.64	0.49	0.23	0.19	0.61	0.6	0.25	0.78
P_2O_5	0.07	0.15	0.08	0.09	0.1	0.1	0.1	0.09	0.09	0.11	0.11	0.77	0.16
LOI	1.31	9.3	10.37	8.71	0.96	1.48	1.02	0.86	0.76	1.65	1.58	8.44	0.88
Total	100.2	98.48	98.97	100.6	100.4	100.8	100.2	100	99.41	100.7	98.77	99.57	99.74
LFSE (ppm)													
Cs	1.8	<0.5	<0.5	<0.5	<0.5	0.6	0.5	< 0.5	< 0.5	0.6	< 0.5	<0.5	0.7
Rb	21	7	12	9	4	15	12	7	4	17	16	8	34
Ba	42	109	135	125	45	138	83	69	55	104	103	1537	118
Sr	114	73	94	101	139	155	158	167	142	204	187	760	197
Ga	17	18	12	14	16	14	14	13	16	15	16	19	19
HFSE (ppm)													
Th	0.6	0.6	0.4	0.5	0.3	0.3	0.3	0.2	0.3	0.6	0.6	16.4	2.8
U	0.2	0.2	<0.1	0.1	<0.1	0.1	0.1	< 0.1	< 0.1	0.2	0.2	3.3	0.9
Nb	3	3	2	3	2	3	2	2	2	2	2	8	8
Ta	0.2	0.2	0.2	0.2	0.1	0.3	0.3	0.3	0.3	0.3	0.3	0.5	0.6
Pb	<5	<5	<5	<5	<5	< 5	< 5	< 5	6	< 5	< 5	6	<5
Zr	53	83	51	59	58	56	61	44	60	59	58	192	108
Hf	1.5	2.2	1.2	1.6	1.5	1.2	1.5	1.1	1.4	1.4	1.4	4.3	2.9
Y	22	27	16	17	21	21	20	16	19	20	19	25	25
REE (ppm)													
La	3.9	5.2	4.9	5.3	4.2	3.2	3.4	3.1	3.8	5	5	94.3	13.3
Ce	9.7	13.3	11.1	11.3	10.2	8.4	8.7	7.7	10.1	12	12.1	187	30.2
Pr	1.42	1.92	1.62	1.52	1.52	1.2	1.29	1.12	1.5	1.53	1.57	21.4	3.97
Nd	7.1	9.4	7.4	6.8	7.5	6.7	6.7	6.4	7.9	8	8.6	82.6	17.1
Sm	2.3	3.1	2.2	1.9	2.5	2.1	2.3	2	2.5	2.2	2.5	14.9	4.7
Eu	1	1.1	0.81	0.68	1.03	0.89	0.87	0.85	0.8	0.94	0.98	3.71	1.58
Gd	3.2	4.2	2.5	2.5	3.1	2.9	3	2.5	3.4	2.8	3.1	10.2	4.9
Tb	0.7	0.8	0.4	0.5	0.6	0.5	0.6	0.4	0.5	0.5	0.6	1.2	0.9
Dy	4.3	5	2.7	3	4	3.6	3.6	3	3.6	3.4	3.6	5.4	5.2
Ho	0.9	1	0.5	0.6	0.8	0.7	0.8	0.6	0.8	0.8	0.8	0.9	1
Er	2.7	3.1	1.6	1.9	2.5	2.1	2.2	2	2.3	2.2	2.2	2.1	3
Tm	0.41	0.48	0.25	0.28	0.37	0.33	0.33	0.3	0.33	0.32	0.34	0.27	0.44
Yb	2.6	3.2	1.6	1.9	2.6	2.2	2.1	2	2.1	2.2	2.2	1.7	2.8
Lu	0.43	0.48	0.26	0.28	0.39	0.34	0.34	0.31	0.33	0.36	0.34	0.24	0.41

Analytical Methods

Major, REE and other trace element composition of selected mafic and felsic volcanic and intrusive rocks from both the Baghmara and Bilari domains have been analyzed, and the data are presented in tables 1A and 1B. Sample locations are shown in figure 1C. Thirteen samples of mafic rocks including four of pillow basalt (BgM1–BgM4), seven of massive basalt (BgM5–BgM11), one each of gabbro and dolerite (BgM12 and BgM13), and seven samples of intermediate to acidic rocks including four of granitoid rocks (BgF1–BgF4), two of ignimbrite (BgF5, BgF6) and one of diorite (BgF7), from the Baghmara domain were analyzed. On the other hand, seventeen samples from the Bilari domain were analyzed which include three of massive basalt (BlM14–BlM16), one of ocellar basalt (BlM17), three of gabbro (BlM18–BlM20), one

TABLE 1A
(continued)

	BgM1	BgM2	BgM3	BgM4	BgM5	BgM6	BgM7	BgM8	BgM9	BgM10	BgM11	BgM12	BgM13
Transition metal (ppm)													
Cr	540	280	360	220	350	200	250	360	210	110	90	120	180
Co	50	56	30	39	52	43	40	49	47	44	42	32	60
Ni	180	140	70	70	150	100	100	150	110	60	60	80	80
Sc	43	40	33	33	39	41	46	43	36	35	36	18	41
V	290	319	233	247	281	276	312	285	286	320	339	162	335
Cu	210	80	60	80	100	50	< 10	160	220	180	190	50	170
Zn	70	110	60	80	80	80	80	90	100	90	90	80	110
Mg#	46.62	40.58	55.78	54.61	48.84	52.82	52.53	48.46	51.08	42.58	42.46	54.5	40.71
Al_2O_3/TiO_2	17.46	11.42	15.68	16.03	14.89	14.15	13.24	15.45	13.35	14.33	12.98	14.39	8.45
Zr/Y	2.41	3.07	3.19	3.47	2.76	2.67	3.05	2.75	3.16	2.95	3.05	7.68	4.32
Zr/Hf	35.33	37.73	42.5	36.88	38.67	46.67	40.7	40	42.9	42.14	41.43	44.65	37.24
Zr/Sm	23.04	26.77	23.18	31.05	23.2	26.67	26.52	22	24	26.82	23.2	12.89	22.98
Ti/Zr	109.9	94.77	96.04	92.97	103.7	104.2	108.4	138	111.7	113.5	120.5	32.3	85.2
La/Sm_{cn}	1.06	1.05	1.39	1.74	1.05	0.95	0.92	0.97	0.95	1.42	1.25	3.95	1.77
Gd/Yb_{cn}	1.00	1.06	1.26	1.06	0.96	1.07	1.16	1.01	1.31	1.03	1.14	4.85	1.42
La/Yb_{cn}	1.02	1.10	2.08	1.89	1.09	0.99	1.1	1.05	1.23	1.54	1.54	37.68	3.23
Eu/Eu*	1.13	0.93	1.05	0.95	1.13	1.1	1.01	1.16	0.8	1.2	1.1	0.87	1.00
Ti/Ti*	0.8	0.89	1.01	1.01	0.91	1	1.02	1.25	1.06	1.17	1.06	0.37	0.9
Sr/Sr*	1.12	0.53	0.84	0.92	1.29	1.69	1.69	1.95	1.30	1.68	1.49	0.47	0.69
Zr/Zr*	0.78	0.91	0.74	0.96	0.79	0.88	0.92	0.73	0.79	0.83	0.74	0.31	0.71
Nb/Nb*	0.39	0.36	0.32	0.41	0.41	0.68	0.44	0.59	0.43	0.25	0.25	0.04	0.24
Ce/Ce*	1.01	1.03	0.97	0.98	0.99	1.05	1.02	1.01	1.04	1.06	1.06	1.02	1.02
CIA	52.22	56.98	48.74	58.94	49.78	50.83	52.35	52.24	49.23	53.55	52.7	54.5	51.12
W'	3.72	3.31	3.34	3.76	3.08	3.59	3.51	3.07	2.97	3.73	3.72	3.91	3.12

of hornblendite (BlM21), three of diorite (BlF8–BlF10), four of rhyolite (BlF11–BlF14) and one each of agglomerate matrix and volcaniclastic tuff (BlF15 and BlF16). Both major and trace element abundances were estimated from powdered rock chips at Activation Laboratories (Ontario, Canada). Fused samples were diluted and analyzed by PerkinElmer Sciex ELAN 6000, 6100, or 9000 inductively coupled plasma mass spectrometry (package 4Litho; details at http://www.actlabs.com). FeO was estimated separately by conventional titration (Process 4Fe-FeO, Actlabs). Detection limits are on the order of 0.01 % for major oxides, except for Mn and Ti, where they are on the order of 0.001 %. For rare earth elements (REEs), the detection limit is 0.04 to 0.1 ppm; for other trace elements, it varies between 0.5 and 5 ppm, except for Cr (20 ppm), Ni (20 ppm) and Zn (30 ppm).

RESULTS

Geology of the SGB

The lower metabasalts dominated unit of the Sonakhan Group, with intrusives of granite, gabbro, and dolerite, is well exposed at and around Baghmara in the western part of the SGB. In contrast, a similar horizon of metabasalts, with interlayered rhyolites and intrusives of gabbro, diorite, and hornblendite, is outcropped at and around Bilari in the eastern part of the belt. The NNW-SSE belt of metasedimentary rocks of the Arjuni Formation, exposed along both the flanks of the Jonk River, subdivides the SGB into western and eastern outcrops, which hereafter would be referred to as the Baghmara and Bilari domains, respectively (fig. 1C).

The Baghmara domain is dominated by massive through pillowed to vesicular metabasalt with local development of lenses of basaltic pillow breccia. Sills and dikes of felsic porphyry are also common in this domain. Phenocrysts of quartz and feldspar

TABLE 1B

Major and trace element composition of mafic lavas and intrusives of Bilari domain

	BlM14	**BlM15**	**BlM16**	**BlM17**	**BlM18**	**BlM19**	**BlM20**	**BlM21**
SiO_2	51.19	55.22	52.12	56.24	47.84	47.63	49.41	59.4
Al_2O_3	16.54	17.26	14.75	13.06	9.2	8.64	18.47	13.82
TiO_2	0.715	1.154	0.811	1.695	0.89	1.049	0.492	1.153
FeO	4.8	7.8	7	3.8	8	8.4	4.6	9.1
Fe_2O_3	0.49	2.08	1.66	12.61	3.28	2.96	2.13	1.78
MgO	2.73	2.75	5.71	1.97	13.35	13.32	6.12	2.67
MnO	0.099	0.085	0.133	0.165	0.164	0.157	0.112	0.137
CaO	7.95	2.42	8.52	0.75	12.2	12.38	9.43	4.67
Na_2O	5.17	3.02	2.14	0.03	1.35	1.17	2.24	2.88
K_2O	1.14	2.16	1.2	1.98	0.77	0.68	2.22	0.79
P_2O_5	0.14	0.21	0.17	0.42	0.41	0.06	0.27	0.2
LOI	7.92	5.21	4.74	7.34	1.95	1.76	2.55	3.01
Total	99.43	100.2	99.73	100.5	100.3	99.14	98.57	100.6
LFSE (ppm)								
Cs	2.5	3.9	1.6	1.3	< 0.5	< 0.5	1.4	<0.5
Rb	40	85	24	91	17	14	71	13
Ba	535	722	458	421	235	201	521	813
Sr	554	217	582	32	400	380	704	177
Ga	14	23	15	22	11	11	15	19
HFSE (ppm)								
Th	5.4	11.8	6.3	19.8	2.3	1.9	3	25.1
U	1.7	3.4	1.7	5.4	0.7	0.4	0.8	3.9
Nb	4	8	5	12	3	3	3	15
Ta	0.4	0.6	0.3	1.1	0.3	0.3	0.3	1
Pb	12	7	7	13	< 5	< 5	6	11
Zr	99	155	109	221	61	53	69	287
Hf	2	3.7	2.7	5.2	1.6	1.4	1.4	6.7
Y	16	26	17	38	20	22	13	46
REE (ppm)								
La	20.4	32.2	24.3	43.6	20.9	12.1	20.4	79.3
Ce	41.9	63.2	48.3	78	43.8	32.1	42.8	139
Pr	4.85	7.32	5.67	9.07	5.53	4.39	5	14.3
Nd	19.1	27.1	20.5	34.3	23.9	22.5	21.7	46.3
Sm	3.8	5.4	3.9	7.6	5.5	5.9	4.7	9.1
Eu	1.14	1.44	1.24	1.75	1.42	1.63	1.68	1.79
Gd	3.4	4.8	3.3	7.4	5.4	5.4	4.1	7.8
Tb	0.5	0.8	0.5	1.3	0.8	0.8	0.5	1.4
Dy	3.1	4.7	3.2	7.6	4.1	4.7	2.7	8.6
Ho	0.6	0.9	0.6	1.5	0.8	0.9	0.5	1.7
Er	1.7	2.7	1.9	4.4	2.1	2.4	1.5	5.1
Tm	0.25	0.38	0.27	0.65	0.3	0.34	0.21	0.74
Yb	1.5	2.5	1.8	4.3	1.9	2.1	1.3	4.9
Lu	0.24	0.38	0.28	0.68	0.28	0.31	0.2	0.78

including plagioclase of albite–oligoclase composition in these rocks indicate their dacitic affinity (after de Wit and Ashwal, 1995). The metabasalts are associated with BIF-ferrugenous shale and greywacke-black shale. Locally, ignimbrite patches are intercalated with the greywacke-shale. In contrast, an assemblage of felsic and mafic lavas and tuffs and intermediate to acidic intrusives constitute the Bilari domain. Small stocks of gabbro and diorite, though infrequent, are common in both the domains. Moreover, an outcrop of metagabbro and metadiorite belonging to the Bilari domain is juxtaposed against the metabasalts of the Baghmara domain along its thrust contact with the Arjuni Formation, at an area NNW of Arjuni village (fig. 1C), implying that the latter metasedimentary unit is disposed, in part, overlapping the junction between the two former metaigneous rock dominated domains.

TABLE 1B
(continued)

	BlM14	BlM15	BlM16	BlM17	BlM18	BlM19	BlM20	BlM21
Transition metal (ppm)								
Cr	180	<20	480	<20	620	600	150	<20
Co	30	28	42	33	55	54	27	40
Ni	80	<20	210	<20	230	250	60	<20
Sc	22	19	26	32	50	55	25	27
V	149	204	175	365	284	303	114	212
Cu	70	<10	50	<10	100	100	40	110
Zn	50	100	70	90	80	70	70	80
Mg#	48.15	33.64	54.51	18.82	68.48	68.21	62.6	30.78
Al_2O_3/TiO_2	23.13	14.96	18.19	7.71	10.34	8.24	37.54	11.99
Zr/Y	6.19	5.96	6.41	5.82	3.05	2.41	5.31	6.24
Zr/Hf	49.5	41.89	40.37	42.5	38.13	37.86	49.29	42.84
Zr/Sm	26.05	28.7	27.95	29.08	11.09	8.98	14.68	31.54
Ti/Zr	43.3	44.6	44.6	46	87.5	119	42.7	24.1
La/Sm_{cn}	3.35	3.72	3.89	3.58	2.37	1.28	2.71	5.44
Gd/Yb_{cn}	1.83	1.55	1.48	1.39	2.3	2.08	2.55	1.29
La/Yb_{cn}	9.24	8.75	9.17	6.89	7.47	3.91	10.66	10.99
Eu/Eu*	0.97	0.87	1.06	0.72	0.8	0.88	1.17	0.65
Ti/Ti*	0.68	0.73	0.78	0.68	0.53	0.63	0.43	0.43
Sr/Sr*	1.50	0.39	1.39	0.05	0.98	1.15	1.80	0.16
Zr/Zr*	0.66	0.73	0.69	0.79	0.31	0.27	0.39	0.79
Nb/Nb*	0.06	0.06	0.07	0.06	0.09	0.12	0.08	0.05
Ce/Ce*	1.03	1.01	1.01	0.96	0.99	1.08	1.04	1.01
CIA	53.7	69.43	55.43	82.55	39.12	37.78	57.08	62.37
W'	3.67	7.33	4.38	27.61	5.16	3.4	3.38	4.68

All the primary planar structures including basaltic flow layers, sedimentary strata and secondary planar fabrics (schistosity or disjunctive cleavage) including plane of flattening of pillows have overall NNW–SSE strike and steep westerly dip. The Baghmara domain of rocks record early reclined folds (F_1), with vertical to steeply westward dipping axial planes, and later upright folds (F_2), with gentle NNW-SSE plunging axis. Rocks of the Bilari domain also show folds which are very similar in geometry to the F_2 folds of the Baghmara domain. Similarly, folds within the Arjuni Formation are of F_2 style, with a westsouthwest-dipping axial plane cleavage, parallel to the plane of flattening in conglomeratic units. There are a number of NNW–SSE thrust faults (fig. 1C), and one along the western boundary of the Arjuni Formation with the Baghmara domain, in particular, is marked with the development of tectonic mélange consisting of foliated cataclasite derived from sandstone, mylonitized felsic porphyry, and gabbroid and basaltic patches, all locally marked by slickensides (Saha and others, 2004).

Succession across Jonk River.—The lithologic succession of the Baghmara domain is well exposed in the Jonk River bed and detailed traverse mapping along E–W lines across the Jonk River bed north of Sonakhan (N21° 30' 47.6": E82° 35' 47.9" to N21° 30' 22.4": E82° 35' 59.5") reveals three successive flows, each marked by pillow lava horizon in the lower part (fig. 2). Taking tight folding of the rocks into account the thicknesses of the lower, middle, and upper flows have been estimated as 25 m, 39 m, and 17 m, respectively, and the thickness of individual flows vary laterally (fig. 2). The pillow forms and their stacking indicate general eastward stratigraphic top (fig. 3A), though there is local reversal due to outcrop scale folds. Each pillow lava layer is preceded by massive basalt or a discontinuous mafic tuff layer and followed successively by massive basalt and then pillow breccia (fig. 2), indicating repetitive cycles of

TABLE 1C

Major and trace element composition of Intermediate to acidic rocks in Baghmara and Bilari domains

	Baghmara domain							Bilari domain								
	BgF1	**BgF2**	**BgF3**	**BgF4**	**BgF5**	**BgF6**	**BgF7**	**BIF8**	**BIF9**	**BIF10**	**BIF11**	**BIF12**	**BIF13**	**BIF14**	**BIF15**	**BIF16**
SiO_2	62.69	62.62	63.13	62.65	74.56	71.71	61.48	50.64	51.14	48.26	66.66	55.37	69.83	68.54	63.53	64.33
Al_2O_3	14.73	14.47	14.05	13.93	13.33	13.91	14.25	14.41	15.71	15.3	14.77	14.5	13.59	12.08	14.92	15.3
TiO_2	0.607	0.62	0.569	0.591	0.153	0.218	0.696	0.663	0.497	1.056	0.252	0.708	0.715	0.562	0.825	0.678
FeO	3.9	4.3	4.4	4.4	1.8	1.8	4.2	8.5	8.3	10.9	1.1	7	2.3	2.8	3.9	1
Fe_2O_3	1.48	1.1	0.89	1.03	0.24	1.07	1.71	0.69	1.01	1.68	2.94	1.27	1.38	0.7	0.95	7.72
MgO	3.79	3.67	3.52	3.71	0.06	0.13	4.15	8.38	6.1	6.24	0.15	5.83	0.44	0.52	0.89	1.79
MnO	0.091	0.085	0.079	0.086	0.03	0.05	0.09	0.15	0.155	0.193	0.078	0.14	0.044	0.08	0.071	0.065
CaO	4.16	4.79	4.17	4.87	0.48	0.72	5.01	9.58	9.61	9.13	2.41	8.77	0.49	2.95	3.8	0.08
Na_2O	3.79	3.53	3.48	3.27	3.84	4.17	3.41	1.91	2.42	2.7	4.78	2.65	2.02	2.83	3.58	0.08
K_2O	2.65	2.82	2.94	2.79	5.03	4.58	2.92	1.62	1.6	0.4	3.51	1.01	6.93	3.85	3.24	4.37
P_2O_5	0.19	0.18	0.17	0.17	0.02	0.01	0.23	0.26	0.08	0.1	0.06	0.11	0.17	0.17	0.24	0.07
LOI	1.5	1.22	1.48	1.65	0.4	0.71	1.47	2.71	2.13	2.79	3.22	2.3	1.1	3.38	4.47	4.41
Total	100	99.88	99.38	99.64	100.1	99.28	100.1	100.5	99.68	99.97	100	100.4	99.25	98.77	100.8	100
LFSE (ppm)																
Cs	1	1.4	1.5	<0.5	<0.5	<0.5	2.4	0.8	<0.5	0.7	3.4	<0.5	1.3	1.3	3.6	6.2
Rb	81	79	90	69	114	127	105	49	33	14	121	22	160	135	162	184
Ba	862	949	846	945	1256	2212	860	290	764	95	945	616	1976	1068	801	762
Sr	425	493	422	443	53	100	472	488	266	187	208	171	221	156	259	16
Ga	16	17	19	18	19	19	19	15	15	16	21	16	15	15	18	20
HFSE (ppm)																
Th	12.1	13.7	22.5	19.5	35.4	31.8	13.7	5.2	6.7	1.4	24.2	11.5	33.8	27.9	50.4	20.5
U	2.3	1.6	4.1	3.3	6.4	5	2.6	1.2	0.9	0.3	6.5	1.4	9.7	8.6	11.9	8.4
Nb	8	8	9	9	17	10	10	3	4	3	11	8	15	14	21	13
Ta	0.9	0.7	0.7	0.8	1.6	0.6	0.8	0.3	0.3	0.1	1.1	0.5	1.4	1.2	2.1	1.4
Pb	17	15	21	20	36	27	22	7	6	<5	36	7	43	47	48	8
Zr	209	184	217	221	332	434	233	76	86	62	267	146	273	224	379	146
Hf	4	3.6	5.3	5	7.7	9.4	5.5	2	2	1.6	5.9	3.4	5.7	4.7	9	3.6
Y	17	16	18	19	35	26	19	18	21	22	37	25	38	32	43	29
REE (ppm)																
La	49.6	55.2	62.6	54.1	136	83.5	54.2	25.3	26.1	9.2	67.2	41	63.8	63.2	97.9	43.3
Ce	93.2	103	118	98.3	240	169	107	54.4	45	20.1	120	70.8	120	114	175	77.7
Pr	9.64	10.4	12.7	10.8	24.6	16.8	12.2	7.03	4.9	2.63	13.3	7.37	11.9	11.2	18.6	8.59
Nd	37.2	37.7	42.5	38.6	80.2	57.2	44	28.5	16.5	11.2	46.5	24.8	43.8	40.1	62.7	29.2
Sm	6.6	6.5	7.6	7.2	12.8	9.8	7.9	6.1	3.4	2.9	8.9	4.7	7.8	7.3	11.2	6
Eu	1.67	1.59	1.69	1.63	1.61	2.78	1.87	1.83	1.05	1.03	1.81	1.19	1.5	1.36	2.43	1.24

TABLE 1C
(continued)

	Baghmara domain							Bilari domain								
	BgF1	**BgF2**	**BgF3**	**BgF4**	**BgF5**	**BgF6**	**BgF7**	**BlF8**	**BlF9**	**BlF10**	**BlF11**	**BlF12**	**BlF13**	**BlF14**	**BlF15**	**BlF16**
REE (ppm)																
Gd	5.1	4.8	4.9	4.9	8.4	6.3	5.3	5.4	3.3	3.5	7	4.3	7.3	6.5	8.8	5.4
Tb	0.7	0.6	0.7	0.7	1.3	1	0.8	0.7	0.6	0.7	1.1	0.8	1.2	0.9	1.4	0.9
Dy	3.5	3.2	3.8	3.9	7.3	5.2	3.9	4.2	3.6	4.2	6.7	4.9	6.8	5.5	1.4	5.7
Ho	0.6	0.6	0.7	0.7	1.3	0.9	0.7	0.7	0.7	0.9	1.3	1	1.3	1.1	1.6	1.1
Er	1.7	1.6	1.9	1.9	3.8	2.6	2.1	2	2.2	2.6	3.8	3	3.9	3.1	4.7	3.3
Tm	0.24	0.24	0.27	0.28	0.55	0.38	0.29	0.27	0.33	0.36	0.58	0.46	0.56	0.44	0.67	0.5
Yb	1.5	1.5	1.8	1.7	3.6	2.7	1.8	1.7	2.2	2.5	3.9	3	3.5	2.8	4.5	3.3
Lu	0.23	0.23	0.27	0.27	0.53	0.41	0.3	0.29	0.35	0.39	0.58	0.45	0.52	0.44	0.7	0.5
La	49.6	55.2	62.6	54.1	136	83.5	54.2	25.3	26.1	9.2	67.2	41	63.8	63.2	97.9	43.3
Transition metal (ppm)																
Cr	170	230	180	190	<20	<20	240	280	420	310	<20	210	30	60	30	190
Co	18	18	18	18	<1	1	22	46	40	40	<1	38	7	4	7	26
Ni	50	50	60	60	<20	<20	60	120	80	90	<20	70	< 20	< 20	<20	90
Sc	13	13	12	13	4	8	13	30	36	34	8	31	10	11	11	20
V	98	97	90	95	<5	<5	111	176	178	193	<5	175	26	25	36	136
Cu	30	30	20	30	<10	10	30	100	40	50	<10	190	< 10	10	<10	20
Zn	60	70	50	70	<30	50	60	80	60	80	80	80	50	60	60	60
A/CNK	0.88	0.82	0.85	0.81	1.06	1.06	0.79	0.65	0.68	0.71	0.92	0.68	1.16	0.85	0.92	3.06
K_2O/Na_2O	0.69	0.79	0.84	0.85	1.31	1.09	0.86	0.85	0.66	0.15	0.73	0.38	3.43	1.36	0.91	54.63
Sr/Y	25.0	30.81	23.44	23.32	1.51	3.85	24.84	27.11	12.67	8.50	5.62	6.84	5.82	4.88	6.02	0.55
La/Sm_{cn}	4.69	5.30	5.14	4.69	6.64	5.32	4.28	2.59	4.79	1.98	4.7	5.45	5.11	5.41	5.46	4.51
Gd/Yb_{cn}	2.75	2.59	2.20	2.33	1.89	1.89	2.38	2.56	1.21	1.13	1.5	1.16	1.69	1.88	1.58	1.32
La/Yb_{cn}	22.46	24.99	23.63	21.62	25.66	21.01	20.46	10.11	8.06	2.49	12	9.28	12.38	15.33	14.78	8.91
Eu/Eu*	0.85	0.84	0.79	0.79	0.45	1.01	0.84	0.96	0.95	0.99	0.7	0.79	0.59	0.59	0.72	0.65
Nb/Nb*	0.14	0.13	0.13	0.15	0.13	0.10	0.16	0.09	0.12	0.32	0.14	0.24	0.13	0.18	0.24	0.18
Ti/Ti*	0.30	0.33	0.29	0.30	0.06	0.07	0.32	0.31	0.39	0.8114	0.1	0.457	0.311	0.273	0.26	0.38
Ba/Ba*	0.91	0.96	0.59	0.8	0.60	1.10	0.75	0.6	1.67	0.71	0.57	1.04	0.87	0.57	0.27	0.41
Sr/Sr*	0.5	0.54	0.41	0.50	0.03	0.07	0.48	0.89	0.67	0.91	0.19	0.28	0.21	0.16	0.17	0.02
Ce/Ce*	1.05	1.05	1.03	0.99	1.02	1.11	1.02	1	0.98	1.002	0.98	0.99	1.07	1.05	1.01	0.99

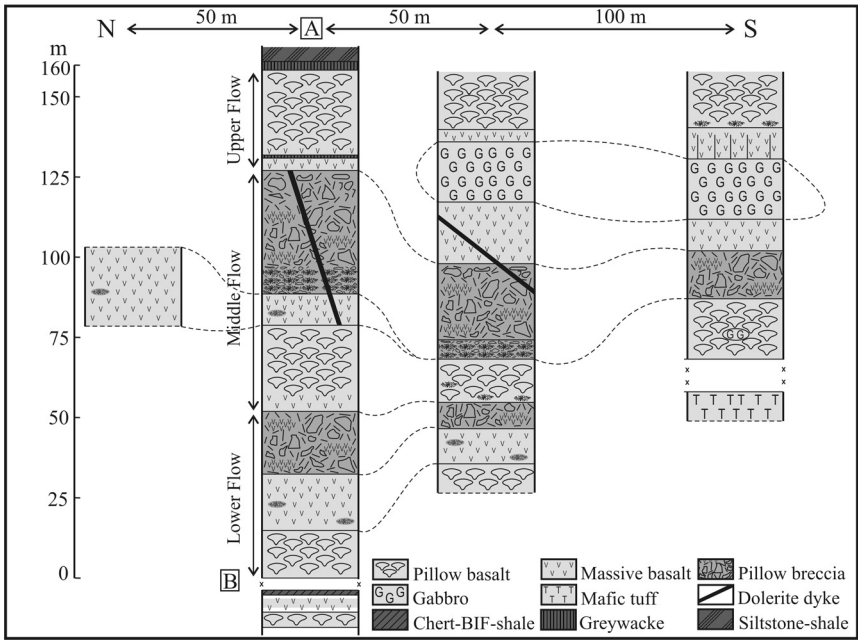

Fig. 2. Lithologs along E-W traverses across Jonk River. Traverse A (N21° 30' 47.6": E82° 35' 47.9") to B (N21° 30' 22.4": E82° 35' 59.5") as marked on figure 1C. Note three cycles of pillow basalt flows, overlain by massive basalt and followed by pillow breccia. Sedimentary intervals are thin.

eruption. The massive basalt layers are locally marked by patches of pillow breccia, whereas the layers of the latter usually contain entrapped lenses of the former. Secondly, each pillow breccia layer shows decrease in fragment size as well as number of entrapped lenses of massive basalt towards the upper part (fig. 3B). Furthermore, the massive basalt of the upper flow in the southern part shows both vertical and horizontal sets of joint (figs. 2, 3C). It is also noteworthy that the middle flow is intruded by dolerite dikes in the northern and central parts and by gabbro in the central and southern parts (figs. 3D, 2). At places, the pillowed basalts are cut across by mm-scale veins of epidote and/or secondary carbonate. Besides there are lenses of ignimbrite in the Baghmara domain, interfingering with metagreywacke, and showing color laminated flow banding and relict fiamme parallel to the foliation in the metasedimentary rock (fig. 3E). On the other hand, immediately west of Jonk River there is another cycle of pillow basalt and massive basalt, which is topped by a discontinuous horizon of chert-BIF-shale (fig. 2). The pillows here also indicate eastward right-way-up direction, and thus this western cycle of mafic lava flows possibly represents an older one relative to the former three. Further east an assemblage of felsic and mafic lavas and tuffs and intermediate and acidic intrusives belonging to the Bilari domain occurs. The Bilari mafic lavas are locally pillowed or vesicular. Small ultramafic intrusions, thin siltstone-shale layers and small conglomerate bodies containing, in places, profuse vesicular basalt fragments, are present as the other constituents of this domain.

Intrusives.—There are small granitic and dioritic stocks, syn-F_1 – F_2 in the Baghmara domain and syn- to post-F_2 in the Bilari domain (Saha and others, 2004). Biotite and hornblende bearing granite stocks in the Baghmara domain contain mafic microgranular enclaves (MME), and xenoliths of metabasalt and metagreywacke (max. size 400×20 cm). Locally, the metabasalt xenoliths and MMEs are traversed by veins of fine-grained pink granite. The granitic stocks are internally foliated with

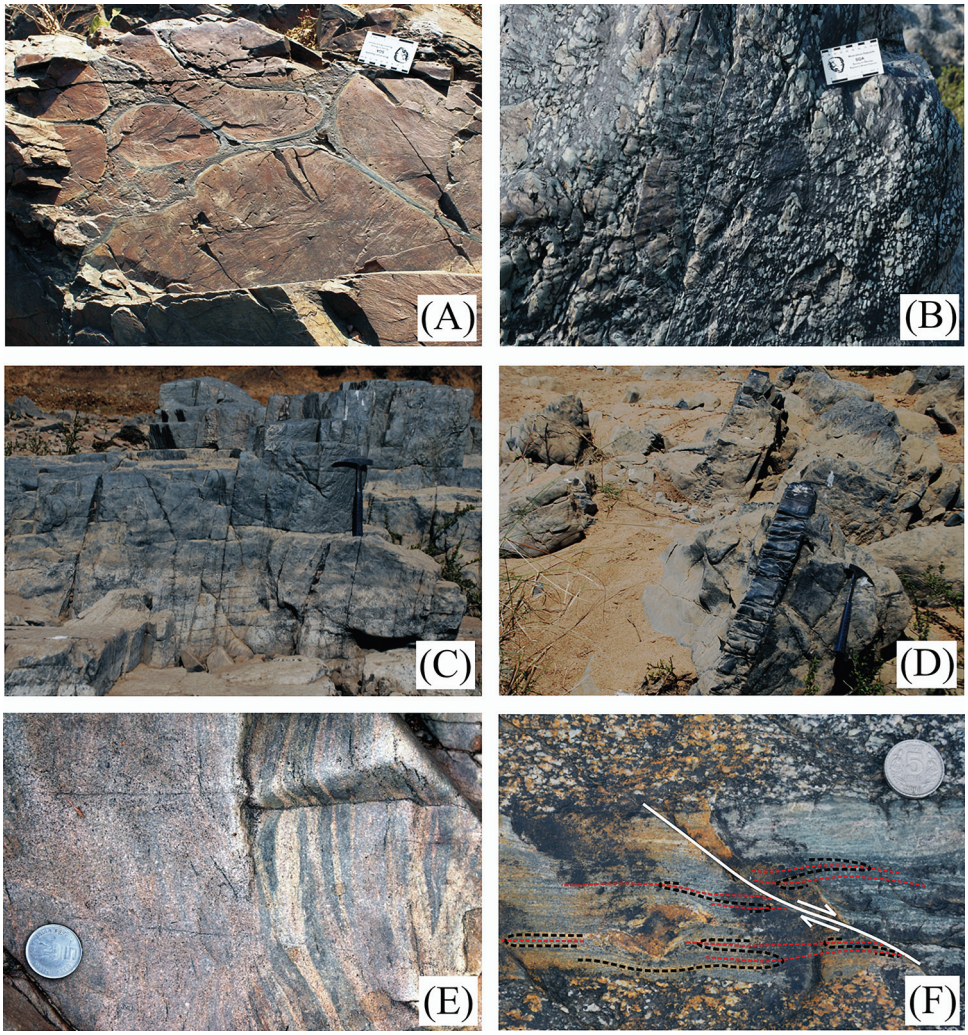

Fig. 3. Field photographs showing (A) convex-up sides of the pillows in the Baghmara basalt indicating eastward right-way-up (towards top of photograph), (B) NNW-SSE trending subvertical pillow breccia layer, with gradual decrease in fragment size from left (west) to right (east) side of the photograph, (C) two perpendicular sets of joint in massive basalt. Length of hammer is 30 cm, (D) dolerite dike across massive basalt/pillow breccia contact. Length of hammer is 30 cm, (E) fiamme and flow bands in felsic ignimbrite, which are parallel to the foliation in the metasedimentary rock . Diameter of coin is 2.3 cm, (F) a raft of greywacke as enclave in granite, Baghmara domain, preserving relict F_1 fold hinges (black discontinuous line) with axial plane (red discontinuous line) parallel to foliation in host granite. Later dextral shear fracture (white line) continues across the contact between the two. Diameter of coin is 2.3 cm, (G) granitic apophyses invading basalt and greywacke layers. Length of pencil is 15 cm, (H) leucocratic (pegmatitic) veins folded as well as boudinaged. Fold axial plane is roughly parallel to foliation in greywacke; boudins suggesting foliation parallel extension. Truncation of fold train possibly due to shearing. Diameter of coin is 2.3 cm, (I) MME with foliation in granite wrapping around it. Diameter of coin is 2.3 cm, (J) metabasalt enclave in diorite. Length of pencil is 15 cm, (K) pebble to boulders of different rock types, set in a sandy matrix. Length of pen is 15 cm, and (L) part of Bouma sequence in greywacke.

parallel alignment of biotite flakes and hornblende needles. Foliation in these stocks is parallel to the F_1 axial plane in the adjoining metagreywacke (fig. 3F). Secondly, there are apophyses of granite, ranging in size from 10×0.3 m to 15×1 m, invading the metabasalt and metasedimentary rocks (fig. 3G). At places, there are thin bands

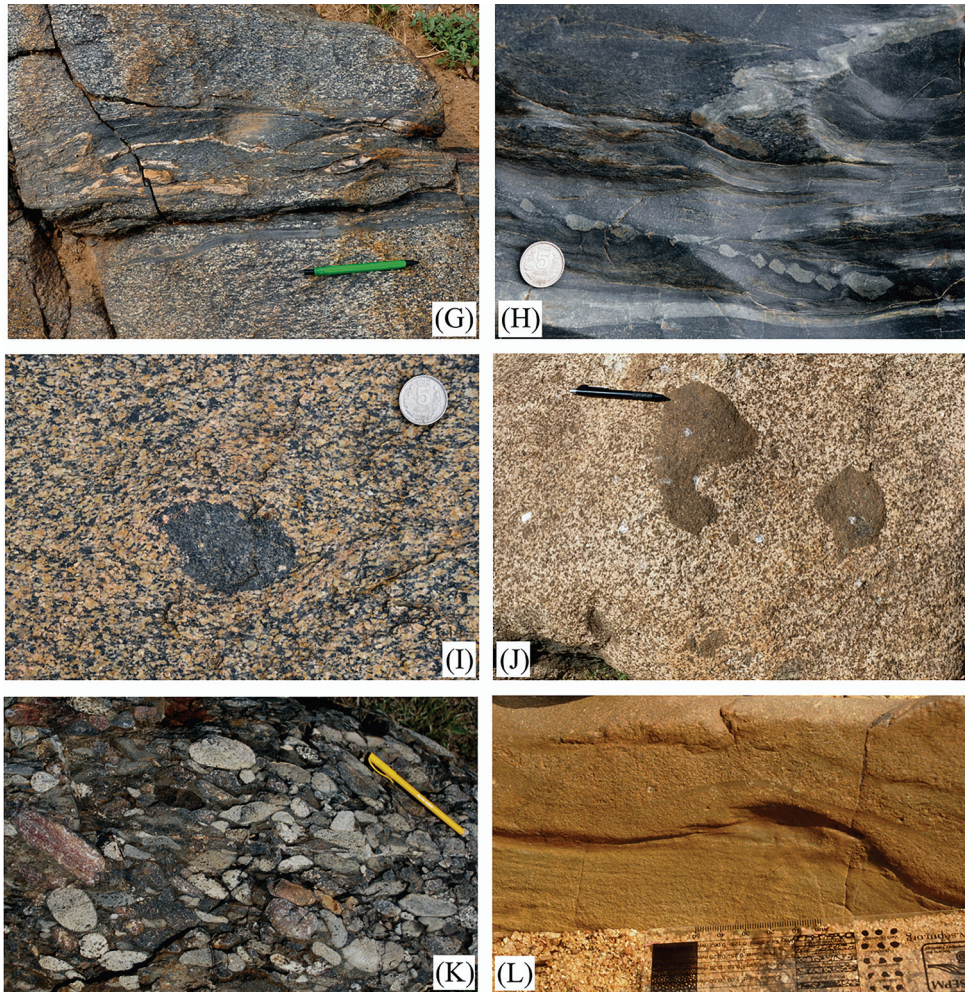

Fig. 3. (continued).

of fine-grained granite along the contact between the coarse-grained granite and metasedimentry rock bands. Although rare, the quartzofeldspathic veins subparallel to or cross-cutting the regional foliation are locally preserved in metagreywacke. These veins at a low angle to regional foliation are strongly boudinaged, while the oblique ones are folded with axial plane subparallel to the foliation (fig. 3H). Locally, subelliptical lenses of metabasalt/MME are aligned parallel to the foliation in the granite, and the internal foliation in these enclaves is oblique to the external regional foliation in the host (fig. 3I). Also, there are conjugate sets of shear planes, oblique to the F_1 axial plane foliation, defining outlines of boudins.

On the other hand, the granitoid bodies occurring as inliers in the Bilari domain are largely granophyric, lack internal fabric, but show circumferential foliation in the contact zone with the metasedimentary country rocks. Similarly, there are rhyolite bodies, interbanded with metabasalts in the Bilari domain, which show foliation near the margin. Furthermore, like the intrusive bodies of granite in the Baghmara

domain, diorite intrusions in the Bilari domain also host enclaves of metabasalt and show crude schistosity wrapping around the enclaves (fig. 3J).

Intercalated sediments.—Although like the metaigneous rocks the sedimentary rocks are also metamorphosed and show weak to strong development of foliation, some original sedimentary characters are still recognizable. A few meters thick discontinuous sedimentary horizon at the top of the pillowed to massive mafic volcanic succession, exposed west of the Jonk River, comprises thin bedded chert, BIF, interbanded with mm- to cm-scale layers of black shale and mafic tuff, all of which show persistent plane parallel lamination. The volcanic succession of the Baghmara domain, exposed in the Jonk River, is followed towards east by massive, thin bedded, immature and normally graded greywacke, overlain successively by siltstone and green-black shale. Farther east within the Bilari domain, there are siltstone-shale patches which are characteristically very similar to the latter sedimentary succession.

The Arjuni Formation separating the volcanic rock assemblages of the Baghmara and Bilari domains consists dominantly of conglomerate-greywacke heterolithic turbidite association, which is, locally, overlain by a thin shale-chert pelagic deposit, with a gradational contact relation in-between.

Conglomerate to heterolithic facies.—In the matrix supported polymictic conglomerate (Jonk conglomerate of Das and others, 1990), layers are tens of centimeter to a few meters thick and are interbanded with thinner greywacke-mudstone units (tens of centimeter). The rounded pebbles to boulders of granite, basalt, vein quartz, BIF, bedded chert, bedded quartzite and siltstone-shale are set in a coarse- to medium-grained sandy matrix (fig. 3K). The conglomerate is on the whole massive and commonly contains outsized clasts, with occasional lenses of massive to trough cross stratified coarse to gritty poorly sorted sandstone. In the interbanded greywacke-mudstone units Bouma divisions are present, where massive to plane laminated grey to off-white greywacke in the lower part grades upward into fine grained rippled or plane laminated (with graded bedding) sandstone and then to mudstone with load casts (fig. 3L).

Pelagic facies.—The pelagic deposit is represented by shale-chert-acidic tuff intervals, east of the conglomerate-greywacke intercalation. Locally, in the vicinity of the thrust contact between the Arjuni Formation and Baghmara domain, it is brecciated, preserving the angular to rounded fragments of bedded chert and tuff in individual beds.

Geochemical Results

Mafic rocks.—The metamorphosed SGB mafic volcanic rocks from both the domains are essentially composed of actinolite, plagioclase, epidote, titanite, and minor chlorite, and rare fresh samples exhibit clinopyroxene phenocrysts set in an intergranular matrix of plagioclase, clinopyroxene and titanite. The gabbro and dolerite have similar mineral assemblage, whereas hornblendite is made up of hornblende, minor plagioclase and titanite. Major and trace element compositions of these rocks from the Baghmara and Bilari domains are given in tables 1A and 1B, respectively. All these samples are relatively high in TiO_2 content (0.72–1.70 wt%), except one sample of gabbro from the Bilari domain (TiO_2 = 0.49 wt%). However, relative to TiO_2 content HFSE and REE of the volcanic and intrusive rock samples from the two domains show different abundance ranges and co-variation patterns, signifying distinct geochemical characteristics of their respective sources. As demonstrated by the plots in TiO_2 versus Zr, Y and Sm, the volcanic rocks from the Baghmara and Bilari domains of the western and eastern parts of the Sonakhan greenstone belt show distinct trends (figs. 4A, B, C). On the other hand, any correlation of these elements

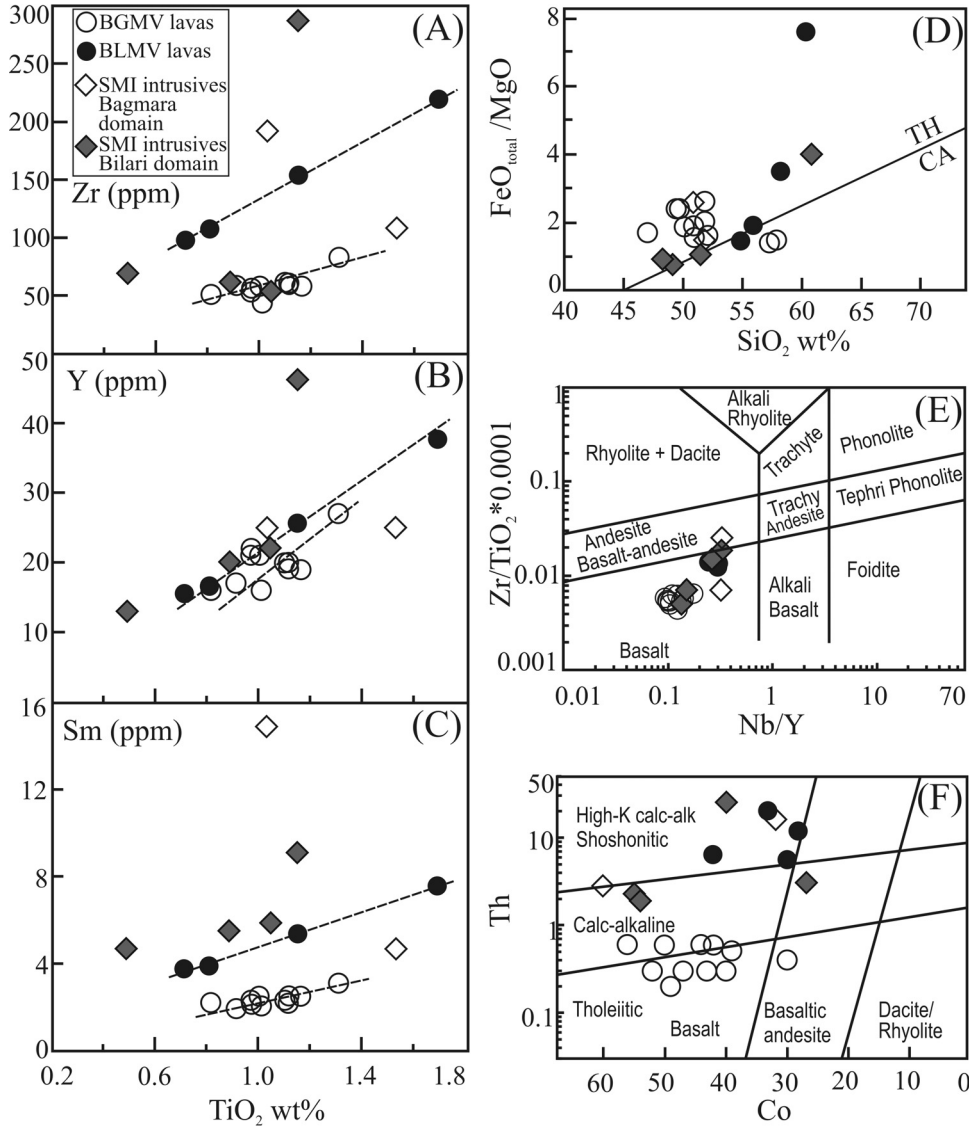

Fig. 4. Major and trace element abundances of mafic rocks of the Sonakhan greenstone belt. (A, B, C) TiO_2 versus Zr, Y, Sm plots, respectively, after O'Neil and others (2011). (D) Plot of SiO_2 versus FeO_{Total}/MgO of lavas of BGMV and BLMV and intrusives of SMI. The boundary line between tholeiitic and calc-alkaline rock types is from Miyashiro (1974). (E) Zr/TiO2 versus Nb/Y (after Winchester and Floyd, 1977) classification diagram for mafic rocks of the SGB. (F) Co versus Th diagram (after Hastie and others, 2007).

is absent in the analyzed samples of mafic intrusives from these domains (figs. 4A, B, C). For convenience, based on these chemical features and location, the samples of the mafic volcanic rocks of the Baghmara and Bilari domains and the mafic intrusives of the SGB are, hereafter, referred to as belonging to the Baghmara Mafic Volcanic (BGMV), Bilari Mafic Volcanic (BLMV) and Sonakhan Mafic Intrusive (SMI) groups.

Major and trace elements.—The Sonakhan mafic rock samples, in majority, are hypersthene normative. However, some samples contain normative hypersthene and

olivine. The BGMV samples are characterized by lower SiO_2 (46.24–53.18 wt%), total alkali (1.49–3.64 wt%) and FeO_{total} (5.77–12.28 wt%), and higher MgO (3.84–7.34 wt%) and CaO (6.72–14.04 wt%) contents than the BLMV ones (wt% of SiO_2: 51.19–56.24, total alkali: 2.01–6.31, FeO_{total}: 5.24–15.02, MgO: 1.97–5.71, CaO: 0.75–8.52). Concentrations of all these oxides in the SMI group are, however, more variable than both the BGMV and BLMV groups. Mg numbers [Mg# = $100Mg/(Mg+Fe_{total})$] for the BGMV, BLMV and SMI group samples range from 40.58 to 55.78 (48.76 on average), 18.82 to 54.51 (38.8 on average) and 30.78 to 68.48 (54.21 on average), respectively. For the BGMV samples the SiO_2, TiO_2, Na_2O and Zr contents correlate negatively, and CaO correlates positively with the MgO values (figs. 5A, B, C, F, H). Furthermore, the FeO_{total}, Al_2O_3, and Ni show positive correlation over the lower ranges of MgO values, and a negative correlation thereafter (figs. 5D, E, G), implying role of crystal fractionation. In contrast, due to lower number of samples such correlations cannot be predicted in case of the BLMV samples. On the other hand, the SMI intrusives show negative correlation of SiO_2 and Na_2O and positive correlation of CaO and Ni with the MgO, and no correlation for the other oxides and elements (figs. 5A–H). The BGMV group shows limited range of Al_2O_3/TiO_2 ratio (13–18), which has large range in both the BLMV (7–23) and SMI (8–38) groups. In comparison to the values of Zr/Y, Zr/Hf and Zr/Sm ratios of N-MORB (2.64, 36 and 28, after Sun and McDonough, 1989) the BGMV shows slightly higher average Zr/Y and Zr/Hf, and lower average Zr/Sm (2.96, 40.44 and 25.13, respectively), whereas the BLMV and SMI groups are characterized by much higher Zr/Y (6.09 and 4.83) and Zr/Hf (43.57 and 41.67) ratios, and slightly or much lower Zr/Sm (27.95 in BLMV and 17.03 in SMI) ratio. And ratios of Ti/Zr (93–121 in BGMV; 43–46 in BLMV and 24–119 in SMI) are generally sub-chondritic.

In FeO_{total}/MgO versus SiO_2 wt% diagram most of the samples of all three groups are plotted in the field of tholeiite, except that two from the BGMV and one from the BLMV groups are plotted just below the calc-alkaline-tholeiite boundary, whereas one each from the BLMV and SMI groups are on the boundary (fig. 4D). Furthermore, plots in Zr/TiO_2 versus Nb/Y and Th versus Co diagrams confirm that the BGMV and BLMV rocks are low-K (0.22–0.64 wt% K_2O) tholeiitic basalts and high-K (1.2–2.16 wt% K_2O) calc-alkaline basaltic andesite, respectively, whereas SMI intrusives with varied K_2O concentrations (0.25–2.22 wt%) range from calc-alkaline basalt to basaltic andesite (figs. 4E, F).

The chondrite-normalized REE profiles for the BGMV group are distinctly different from those for the other groups (figs. 6A, B, C). REE concentrations of the BGMV samples are 10 to 20 times relative to the chondrite values. The near-flat profiles (La/Yb_{cn} = 0.99–2.08) of this group are marked by slightly depleted to enriched LREE patterns (La/Sm_{cn} = 0.92–1.74), slightly negative to positive Eu/Eu* (0.84–1.16) and almost unfractionated HREE with Gd/Yb_{cn} (0.96–1.31, on average 1.1, relative to N-MORB value of 0.998, after Sun and McDonough, 1989). In contrast, both the BLMV and SMI groups show enriched LREE patterns (La/Sm_{cn} = 3.35–3.89 in BLMV and 1.28–5.44 in SMI), negligible Eu anomaly (Eu/Eu* = 0.87–1.06 in BLMV and 0.8–1.17 in SMI) and weakly to moderately fractionated HREE patterns (Gd/Yb_{cn} = 1.39–1.83 in BLMV and 1.29–4.85 in SMI), except the samples of osceller basalt (BlM 17) and hornblendite (BlM 21) from the Bilari domain, which show enriched LREE, small negative Eu-anomalies and almost flat HREE patterns (figs. 6B, C). In N-MORB normalized trace element diagram the BGMV samples show elevated abundances of large ion lithophile elements (LILE, that is, Rb, Ba, Th). It is noteworthy that their relative concentrations of high field strength elements (HFSE, that is, Nb, Ta, Zr, Ti) and of LREE and HREE are close to unity (fig. 6D). However, in spite of near flat abundance pattern of elements, Sr to Lu, these samples present slightly negative to positive Sr

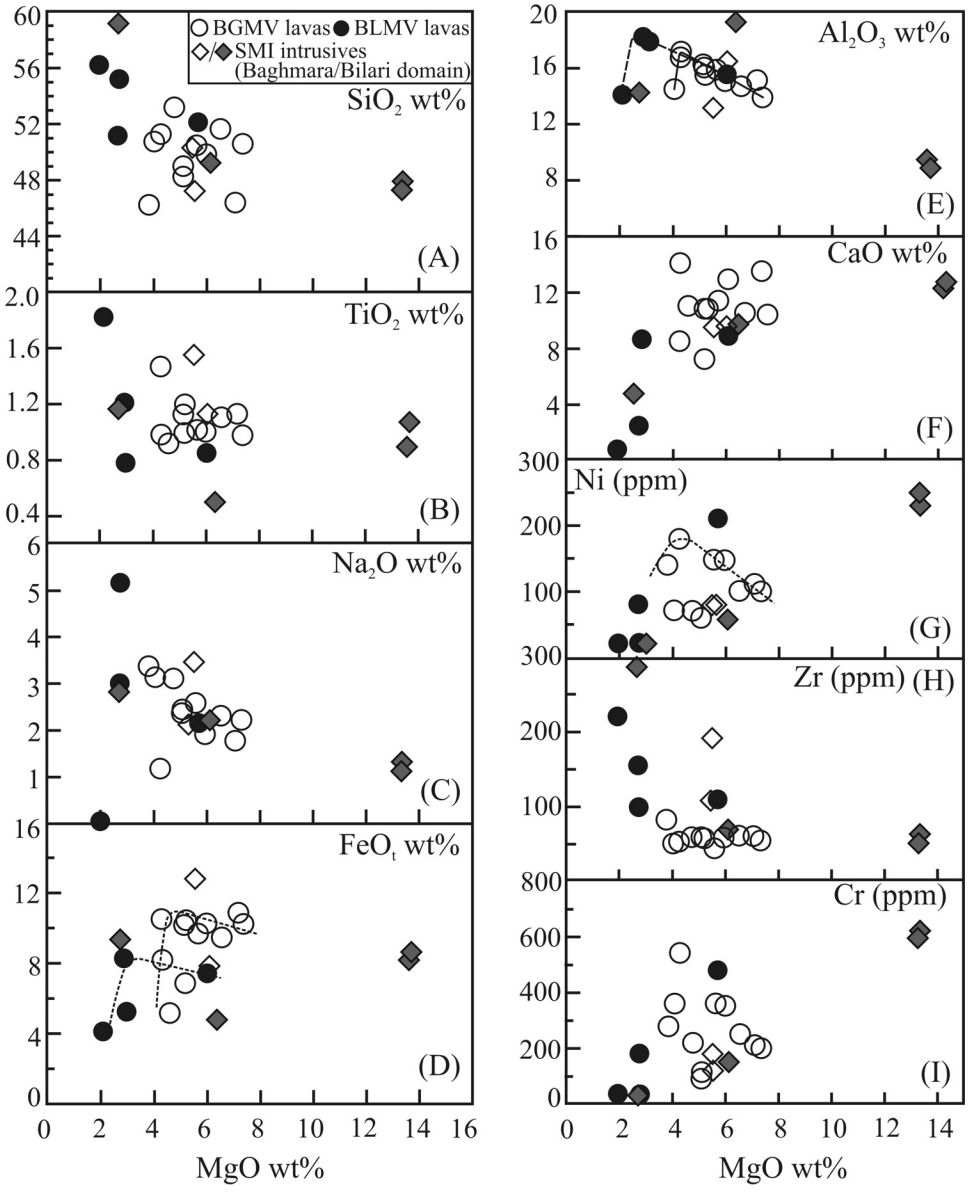

Fig. 5. Plots of major elements and Ni, Zr and Cr against MgO for the SGB mafic rocks.

(Sr/Sr* = 0.51–2.29) and negligible Zr (Zr/Zr* = 0.73–0.96) and Ti (Ti/Ti* = 0.80–1.25) anomalies. In addition, strongly positive K and negative Nb, P and Cr anomalies are there (fig. 6D). In contrast, both the BLMV and SMI rocks are characterized by enrichment of all elements more incompatible than Ti, relative to N-MORB (figs. 6E, F). Additionally, the BLMV samples show large negative Nb/Nb* (0.06–0.08), moderately negative Ti (Ti/Ti* = 0.68–0.78) and P and Cr anomalies (fig. 6E), whereas the SMI group is marked by strongly negative Nb (Nb/Nb* = 0.04–0.24), Zr (Zr/Zr* = 0.31–0.79), Ti (Ti/Ti* = 0.36–0.91) and moderately negative P and Cr anomalies (fig. 6F).

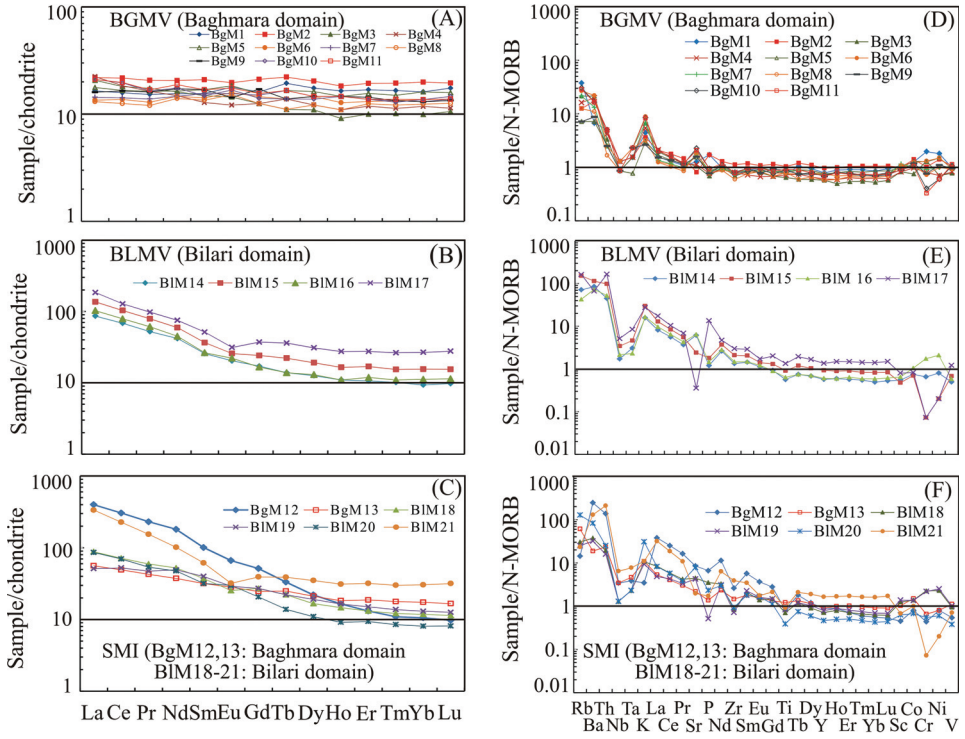

Fig. 6. Chondrite-normalized rare earth element patterns and normal mid-oceanic ridge basalt (N-MORB; Sun and McDonough, 1989) normalized trace element patterns for the SGB mafic rocks. (A, D) BGMV samples, (B, E) BLMV samples, (C, F) SMI samples.

Felsic rocks.—Both the Baghmara and Bilari domains of the SGB have small granitic and quartz dioritic plutons which intrude volcano-sedimentary successions. Besides there are patches of rhyolite, ignimbrite and felsic tuffs, intercalated with the mafic volcanic rocks and sedimentary rocks. The granitoid rocks have quartz + plagioclase + K-feldspar + biotite + hornblende ± titanite ± apatite ± muscovite as constituent minerals, and the mineral assemblage of the dioritic rocks is sodic plagioclase + hornblende + titanite ± quartz ± apatite. On the other hand, because of extremely fine grain size the mineralogy of the felsic volcanic rocks and tuffs could not be assessed properly, however, some of these are quartz and K-feldspar phyric.

Major and trace elements.—With 61.48 to 63.13 wt% SiO_2 contents the felsic plutons show granodioritic An-Ab-Or normative proportion and are calc-alkaline and metaluminous ($0.81 \leq A/CNK \leq 0.88$; fig. 7A, B, C). They are characterized by moderately high total alkali (6.06–6.44 wt%), high K_2O/Na_2O values and low CaO (4.16–4.87 wt%) contents and are low in ferro-magnesian oxides ($5 \leq FeO_{total}+MgO+MnO+TiO_2 \leq 10$ wt%; fig. 7D). The quartz diorites are characterized by a large range of SiO_2 contents, extending down to mafic compositions ($48 \leq SiO_2 \leq 62$ wt%) and have tonalitic normative composition, except one sample (BgF7) with granodioritic norm (fig. 7A). They are calcic to calc-alkaline and strongly metaluminous ($0.65 \leq A/CNK \leq 0.80$; figs. 7B, C) and have variable total alkali (3.1–6.33 wt%) and high CaO (5.01–9.61 wt%) contents. They are also high in ferro-magnesian oxides ($10 \leq FeO_{total}+MgO+MnO+TiO_2 \leq 20$ wt%; fig.7D). Both the granites and quartz diorites

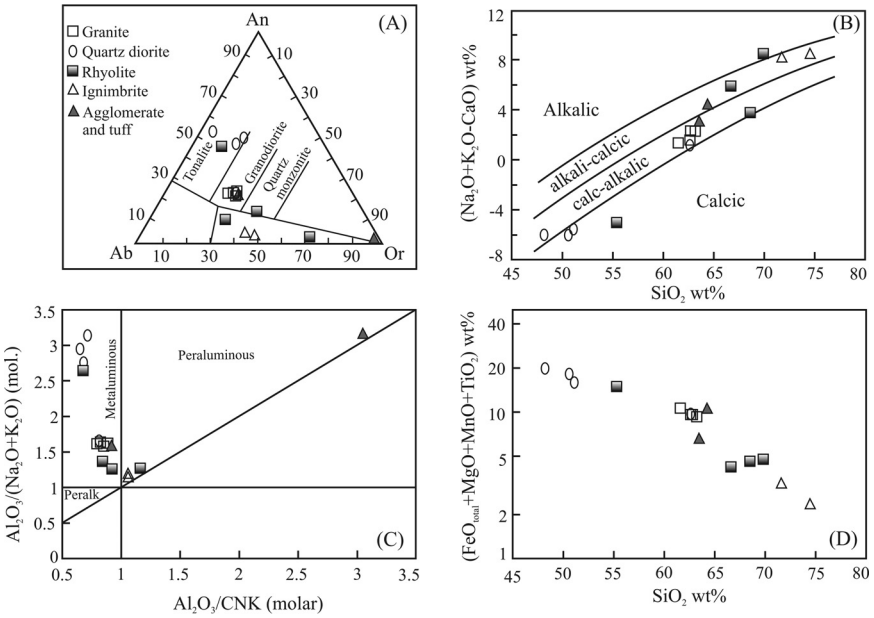

Fig. 7. Major element geochemistry of the intermediate to acid intrusives, lava, agglomerate and tuff, Sonakhan greenstone belt. (A) Classification based on normative composition, after Barker (1979). (B) MALI index ($[Na_2O+K_2O]$–CaO) versus SiO_2 diagram of Frost and others (2001) showing restricted range of composition of granites and diorites, across the boundary between calcic and calc-alkalic rock types, but wide variation of the felsic volcanic rocks, over calcic to alkali fields. (C) A/NK (molar $Al_2O_3/[Na_2O+K_2O]$ ratio) versus A/CNK (molar $Al_2O_3/[CaO+Na_2O+K_2O]$ ratio) diagram after Maniar and Piccoli (1989), samples mostly plot in the field of metaluminous rocks. (D) Sum of "mafic" oxides ($FeO_{total}+MgO+MnO+TiO_2$) versus SiO_2 diagram.

are rich in transition elements including V (90–193 ppm), Ni (50–120 ppm) and Cr (170–420 ppm) contents.

On the other hand, the Sonakhan intermediate to acid volcanic rocks including rhyolite, ignimbrite, agglomerate matrix, and tuff are highly variable in normative composition, ranging from tonalite through granodiorite to granite (fig. 7A). The MALI index of these samples is also variable, reflecting calcic to alkali-calcic or even slightly alkaline characters (fig. 7B). Three rhyolite and agglomerate matrix samples are metaluminous ($0.68 \leq A/CNK \leq 0.92$), ignimbrite and one rhyolite samples have slightly >1 A/CNK (1.06–1.16), whereas the tuff sample is peraluminous (A/CNK=3.06; fig. 7C). Unlike the intrusives, the Sonakhan felsic volcanic rocks are variable in total alkali (3.66–8.87 wt%) and CaO (0.08–8.77 wt%) contents, and high in K_2O/Na_2O values. Furthermore, they are low in ferro-magnesian oxides ($2 \leq FeO_{total}+MgO+MnO+TiO_2 \leq 7$ wt%), except one rhyolite and tuff samples, both containing ~ 8 wt% FeO_{total} (fig. 7D). In contrast to the SGB felsic intrusives, the felsic volcanic rocks are usually poor in V (25–36 ppm) as well as in Ni (< 20–90 ppm) and Cr (< 20–210 ppm) contents. However, the trends of geochemical evolution of all the Sonakhan intermediate to acid intrusives and volcanic rocks as demonstrated by the broadly negative correlation of MgO, MnO, $Fe_2O_3^T$, Al_2O_3, TiO_2, as well as CaO contents with SiO_2 wt%, in the Harker diagrams, are similar, except the granites, which display least variation (Appendix fig. A1).

Chondrite-normalized REE profiles of all the SGB felsic rock samples in general display enriched LREE and flat HREE patterns (figs. 8A, B). Granite samples are characterized by highly fractionated REE (La/Yb_{cn} = 21.62–24.99) patterns, with

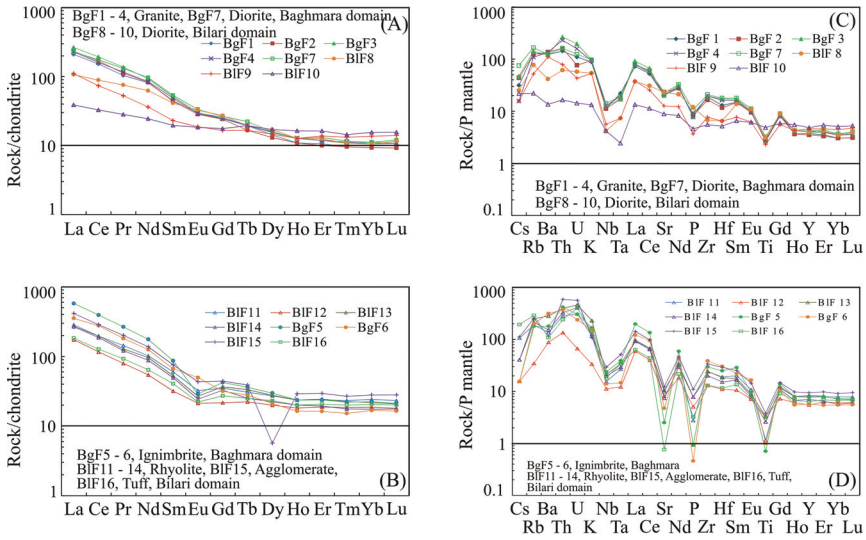

Fig. 8. Trace element geochemistry of the acid to intermediate intrusives, lava, agglomerate and tuff, Sonakhan greenstone belt. Chondrite-normalized rare earth element and primitive mantle (PM; Sun and McDonough, 1989) normalized multi-element patterns. (A, C) for intrusives and (B, D), for volcanic rocks.

moderately high LREE enrichment (La/Sm_{cn} = 4.69–5.30) and near-flat HREE (Gd/Yb_{cn} = 2.20–2.75), whereas the quartz diorites are variably fractionated, with the La/Sm_{cn}, Gd/Yb_{cn}, and La/Yb_{cn} ratios ranging 1.98 to 4.79, 1.13 to 2.56 and 2.49 to 20.46, respectively. On the other hand, the felsic volcanic rocks possess moderately high La/Sm_{cn} (4.51–6.64), very low Gd/Yb_{cn} (1.16–1.88) and variably high La/Yb_{cn} (8.91–25.66) ratios.

All the felsic intrusive and volcanic rocks of the SGB are moderately rich in incompatible elements (1–10 times the primitive mantle values), with LILE (Cs, Rb, Ba)-HFSE (Th, U) enriched convex-upward patterns, negative Ba, Nb-Ta, Sr, P and Ti anomalies (figs. 8C, D) and low Sr/Y ratios. Granites show slightly negative Ba-anomaly (Ba/Ba* = 2*Ba/(Rb+Th) = 0.60–0.96) and moderately negative Sr-anomaly (Sr/Sr* = 2*Sr/(Ce+Nd) = 0.41–0.54). In contrast, quartz diorites have moderately negative to positive Ba-anomaly (0.60–1.67) and moderately to slightly negative Sr-anomaly (0.48–0.91). On the other hand, the felsic volcanic rocks are marked by moderately negative to slightly positive Ba-anomaly (0.27–1.10) and strongly negative Sr-anomaly (0.02–0.28). It is also noteworthy that these volcanic rocks show stronger Nb-Ta-, P- and Ti-anomalies, compared to the intrusive granites and diorites (figs. 8C, D).

DISCUSSION

As the natures of Archean tectonic processes are yet to be fully understood, assessment of tectonic setting of the Sonakhan greenstone belt (SGB) needs caution, particularly on the basis of geochemical comparison with the modern analogues. Here we present an interpretation of tectonic evolution of the Sonakhan greenstone belt based on characteristics of both the metaigneous and metasedimentary assemblages in different domains of the SGB.

Lithologic Association in the SGB

Rock succession and deformation.—Taking into account variations in lithological association, structure, and stratigraphy, the SGB has been divided into four lithotectonic units, presently separated by thrusts. The westernmost unit (oldest) is a succession of massive to vesicular basalt and pillow basalt, topped by chert-BIF-shale, and comparable to the upper part of an ancient oceanic crust (fig. 2). It is followed eastward by the three cycles of massive to pillow basalt flows alternating with pillow breccia, and topped by a thin greywacke-shale unit (fig. 2). The lithological attributes of these metasedimentary rocks associated with the BGMV group rocks of the Baghmara domain, as mentioned earlier, suggest their deposition under the prevailing influence of turbidity current below storm wave base (Bouma, 1962; Walker, 1978; Lowe, 1982; Saha and others, 2017). Furthermore, the interleaving of the pillow basalt and pillow breccia layers, fining-up pillow breccia distribution, formation of joints in the upper volcanic rock layers, interbanding with greywacke in the Jonk River section as well as capping of this whole sequence by the greywacke-siltstone-shale succession of the Bilari domain (figs. 2, 3B, 3C) collectively stand for gradual shallowing-up or cyclic sea-level fluctuation, as reflected in by the successive flows too. On the other hand, the Arjuni Formation is dominated by matrix to clast supported conglomerates and greywacke turbidites (heterolithic facies) grading to siltstone-shale. The conglomerate-greywacke association possibly represents a submarine fan of deep water environment, as is indicated by the lithological attributes, while the siltstone-shale association represents a pelagic to below storm wave base deposit.

Although F_1 folds are not well developed in the BLMV rock outcrops, we consider that the BGMV and BLMV groups of western and eastern parts of the SGB are broadly coeval in deformation history. In contrast, the heterolithic conglomerate horizon of the Arjuni Formation contains pebbles of basaltic and granitic rocks, and quartzite (meta-chert), and records F_2 folds only. Thus, it has been interpreted that towards the waning stage of F_1 folding of the BGMV-BLMV volcanic rocks and associated sedimentary rocks, intrusions of acid to intermediate plutons and sedimentation of the Arjuni Formation took place (Deb, 2013). As mentioned earlier, the contact between the BGMV outcrops of western part (Baghmara domain) and the Arjuni Formation is marked with the foliated sandstone cataclasite, mylonitized felsic porphyry, and patches of gabbroic and basaltic rocks, together with local slickenside. This deformed contact zone of rock slivers of heterogeneous parentage possibly represents a tectonic mélange, reminiscent of accretionary wedges (Xiao and others, 2003; Pound and others, 2014). The gabbroic blocks possibly derived from lower part of the oceanic crust of the western Baghmara domain and mixed with rafts of basalt off-scraped from the upper part of the crust of the eastern Bilari domain in a tectonic mélange.

Alteration, metamorphism and mobility of elements.—The mobility of an element depends upon the extent of water-rock interactions and the elemental solubility under the reaction conditions (Kelley and Delaney, 1987; Bickle and Teagle, 1992). Deformed Precambrian rocks, in particular, are prone to metasomatic and metamorphic alteration, as had been tested with the help of correlation between concentrations of REE and HFSE (Frei and others, 2002; Polat and others, 2000, 2002; Polat and Hofmann, 2003; O'Neil and others, 2011). Similarly, Ce/Ce* values for mafic rocks, ranging 0.9 to 1.1, is considered as the rider representing least alteration (Polat and others, 2002; Mazumder and Arima, 2009; Saha and others, 2017, 2021; Sain and Saha, 2018). On the other hand, CIA, the Chemical Index of Alteration (Nesbitt and Young, 1982), and W′, an empirical statistical index of chemical alteration (Ohta and Arai, 2007), have been widely used to address the question of weathering of rocks.

As mentioned earlier, the Sonakhan mafic rocks, ranging from basalt to basaltic andesite, underwent at least two phases of deformation under greenschist facies conditions. Therefore, assessment of changes in composition caused by complex history of these rocks, if any, becomes important before using chemical signatures to constrain the nature and evolution of the parent magma. Relative to REE the high field strength elements, such as Zr, Nb, Hf, and Th vary in well-correlated trends in all the three groups of the SGB mafic rocks, and the values of correlation coefficient (R) of Zr, Hf and Th with REE like La, Gd, Sm and Nd and Nb are fairly high in the range 0.75 to 0.99, 0.68 to 0.96, 0.61 to 0.97 and 0.63 to 0.97, respectively. Secondly, the Ce/Ce* values for all the analyzed mafic samples of the SGB are consistently close to 1, ranging from 0.95 to 1.07 (tables 1A, 1B). On the other hand, these rocks often show mm- to cm-scale patches and discontinuous veins of epidote and calcite, suggesting that Ca was probably mobile during metamorphism/alteration. The CIA values for the BGMV, BLMV and SMI groups range respectively from 35 to 45, 40 to 79 and 26 to 50 (tables 1A, 1B), out of which, only the BLMV samples have slightly higher values than those typical of fresh basalts (30–45, Nesbitt and Young, 1982). Furthermore, the CIA values of all these analyzed samples collectively show negative correlation with the CaO contents (Appendix fig. A2A), standing against remobilization of Ca by any hydrothermal solution during metamorphism. Moreover, the abundance of pillowed basalts, and relatively high L.O.I. (Loss-on-ignition) contents of a few samples (8–10 %) may be regarded as due to alteration by syn- to post-eruption interaction with seawater. However, the majority ($\sim$ 71 %) of the samples have L.O.I. contents < 5 %, thus giving an indication of only minor alteration, if any. Furthermore, in plots of major element oxides versus L.O.I. (not shown) we did not find any correlation, which might have indicated enrichment or depletion relative to L.O.I. The values of W′ for these samples are low (2.97–7.33; tables 1A, 1B), except in sample BlM 17 (osceller basalt, 27.61), and lack any significant correlation with the Al_2O_3/TiO_2 ratios, Zr contents and Eu-anomaly (Appendix fig. A2B, A2C, and A2D). Thus, we consider that element mobility, if any, during alteration and metamorphism did not change original element concentrations in the analyzed samples to any significant extent. Negative Nb anomalies in the SGB mafic volcanic and intrusive rocks may reflect some crustal contamination. The values of Al_2O_3/TiO_2 ratio (7.71–23.13) and Zr anomaly [$Zr/Zr^* = 2*Zr_{pm}/(Sm_{pm}+Nd_{pm})$ = 0.78–1.13] of the Sonakhan mafic volcanic rocks are either much less or higher than those of continental crust (18 and 0.94 respectively). Moreover, absence of correlation between the magnitude of negative Nb anomalies and contents of SiO_2, MgO, Ni, Cr, Co, Th, Ti and LREE in case of these rocks (tables 1A, 1B) stands against any significant crustal contamination.

Similarly, in case of the SGB felsic rocks L. O. I. contents (0.4–3.4 %), except in agglomerate matrix and tuff samples (4.4–4.5 %), values of the correlation coefficient (R) of Zr with Gd (0.77), Sm (0.84), Nd ((0.84) and Nb (0.81), and the range of Ce/Ce* (0.97–1.1) collectively suggest that these rocks were also not significantly affected by either metamorphic or metasomatic alteration.

Petrogenesis of mafic rocks.—As discussed above, the contribution of either pre-metamorphic alteration or later syn-tectonic metasomatic processes to the chemistry of the Sonakhan metabasic rocks, if any, is negligible. Therefore, we consider abundance and relative proportions of HFSE and REE in the SGB metabasic rocks reflect the primary chemical characters of their parent magmas.

Origin of magma.——As mentioned earlier, the BGMV group represents low-K tholeiitic basalts, the Mg#s of which (on average 48.76) are slightly lower than those of primitive MORB, with average Mg#s of 52.8 to 59.7, from Atlantic, Pacific and Indian ocean spreading centers (Wilkinson, 1982). However, the BGMV group shows

negative correlations of the SiO_2, TiO_2, Na_2O and Zr contents and positive correlation of the CaO values against MgO contents (fig. 5). Furthermore, it presents negative correlation of the FeO_{total} values and positive one of the Al_2O_3 and Ni contents against lower range of MgO values (fig. 5). All these features are comparable to the modern worldwide MORB characteristics, which show decreasing Ti, Mn, Na, P, and increasing Al, Ca, Ni, Cr values with increasing Mg#s (Wilkinson, 1982, Shervais and others, 2019). It is also corroborated by almost flat La – Lu sector of the N-MORB normalized trace element diagram, about the line of unity (fig. 6D). Furthermore, in the MORB plus Ti normalized trace elements diagram after Pearce (2008) these samples show slight Th-Nd enrichment (fig. 9A), reflecting more enriched character of the source relative to that of the N-MORB, like the primitive mantle (PM), and low but varied degrees of partial melting at source. The flat chondrite-normalized REE profiles are generally considered as indicative of origin of the parent magmas from partial melting of a spinel lherzolite source (Aldanmaz and others, 2000; Workman and Hart, 2005). In contrast, the REE patterns with fractionated HREE stand for garnet lherzolite source (Liu and others, 2018). All the BGMV samples show near-flat REE patterns (fig. 6A), with slightly higher $(Sm/Yb)_{cn}$ ratios (on average 1.05) than that of N-MORB (0.96). Moreover, in the Sm/Yb versus La/Sm diagram, the BGMV samples plot along spinel lherzolite melting curve, but close to PM, indicating that their parent magmas may have produced by ~1 to 5 % partial melting of primitive spinel lherzolite source (fig. 9D). Thus, we infer that the low-K tholeiitic BGMV basalts were originated from magmas, derived predominantly from partial melting of a primitive spinel lherzolite mantle source with an N-MORB affinity and minor garnet bearing relics.

However, there is significant overlap in the geochemical signatures of the back-arc basalts with those originating in Mid-Ocean Ridge systems, especially those developing over intra-oceanic subduction systems (Saunders and Tarney, 1984; Wilson, 1989). For example, the Parece Vela basin and Shikoku basin west of (Proto) Mariana arc, as well as early erupted basalts sampled from Mariana trough, are usually olivine normative, and virtually indistinguishable from ocean ridge tholeiites in terms of mineralogy and major element chemistry (Hart, 1971; Hawkins, 1976, 1977; Saunders and Tarney, 1979; Mattey and others, 1980; Wood and others, 1981). In addition, low LILE to HFSE ratios, and trace element patterns very close to that of N-MORB (Sun and McDonough, 1989) underscore the geochemical similarity of relatively early formed back-arc basalts and MORB (Saunders and Tarney, 1984). However, there is considerable variation in the geochemistry of back-arc basalts, particularly those originating as ensialic basins, and due to mantle heterogeneity beneath spreading centres. Thus, the low-K, olivine normative character, N-MORB normalized flat REE pattern, and other trace element signatures in the BGMV samples are equally well explained as representing oceanic back-arc setting. The proximity of the calc-alkaline BLMV domain and the BGMV domain is also consistent with a back-arc origin for the BGMV.

The BLMV and SMI group samples are geochemically similar to calc-alkaline suites. The co-variations of major oxides and trace elements with MgO contents, though in case of the BLMV group similar to that of the BGMV group, due to low sample number and restricted MgO wt% range such correlations are obviously not significant (fig. 5). The SMI group, in contrast, does not possess any such correlation (fig. 5). However, both the BLMV and SMI groups are characterized by E-MORB type REE profiles with enriched LREE and fractionated HREE patterns (figs. 6B, C), enrichment in trace elements more incompatible than Ti, relative to N-MORB, and negative Ti-anomaly (weak in BLMV and strong in SMI; figs. 6E, F), and enriched Th–Ti patterns in MORB plus Ti normalized diagram (figs. 9B, C). Although the alteration effect may influence the abundance of K_2O, the BLMV samples have consistently higher K_2O contents compared to the BGMV samples, and the high LILE to HFSE

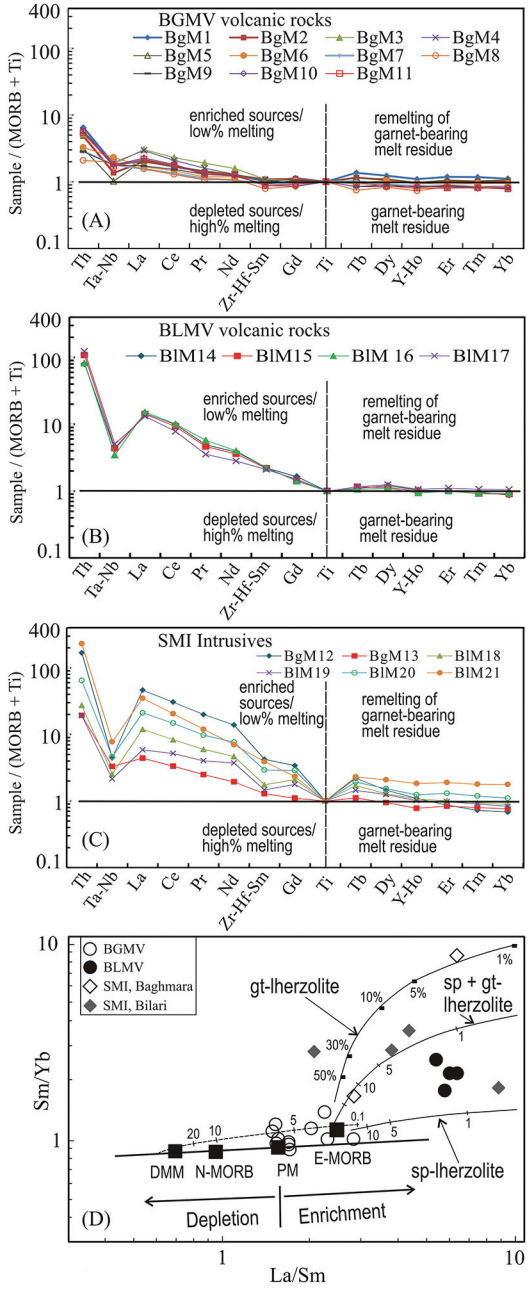

Fig. 9. (A, B, C) (MORB+Ti)-normalized multi-element plots for BGMV, BLMV and SMI groups, respectively, after Pearce (2008). (D) La/Sm versus Sm/Yb diagram of SGB mafic rocks. Garnet and spinel lherzolite melting curves are after Aldanmaz and others (2000); numbers along lines represent the degree of the partial melting. Depleted mantle MORB (DMM), Primitive mantle (PM), normal mid-oceanic ridge basalt (N-MORB), and enriched mid-oceanic ridge basalt (E-MORB) compositions are from Sun and McDonough (1989).

ratio (N-MORB normalized) is reminiscent of arc basalts as in the Mariana arc and Scotia arc (Saunders and Tarney, 1984). All these geochemical characters collectively stand for origin of parent magmas of the BLMV and SMI groups from enriched mantle source at the field of garnet stability. Moreover, in the MORB plus Ti normalized diagram samples from these two groups in general show negative La–Ti trend, persistent for the BLMV group and variable for the SMI group (figs. 9B, C), possibly reflecting variation in either degree of enrichment or of partial melting at the source (Pearce, 2008). In the Sm/Yb versus La/Sm diagram, the BLMV samples plot close to the spinel plus garnet lherzolite melting curve in the region of lherzolite with spinel greater than garnet, indicating origin of the parent magma by ~2 to 3 % partial melting of a sp+gt lherzolite mantle source (fig. 9D). The SMI samples, however, straddle over the melting curves for spinel plus garnet lherzolite and garnet lherzolite, and thus indicate varied ~2 to 30 % partial melting of the source to generate the parent magmas. It is thus apparent that the calc-alkaline BLMV and SMI group rocks originated from magmas, derived predominantly from partial melting of enriched garnet lherzolite mantle source at different depths, shallower and greater for the BLMV and SMI groups, respectively.

Differentiation.——It is well understood that fractionation of basic magma is controlled by mafic phases like olivine and pyroxene in the earlier stages and by plagioclase in the later stages, when Eu, Rb and Ba all may substitute in the cationic sites of plagioclase. As mentioned earlier, both the BGMV and BLMV groups show correlations of Al_2O_3, FeO_{total} and Ni contents with MgO wt%, as positive at lower and negative at higher MgO ranges, implying role of crystal fractionation. Secondly, the analyzed samples of all three groups show enrichment of Rb and Ba and weak to prominent Eu anomaly in MORB and chondrite normalized diagrams (figs. 6A–F), implying the role of plagioclase fractionation during evolution of these magmas. With the help of plots in Al_2O_3 versus SiO_2 and TiO_2 versus SiO_2 diagrams showing experimental plagioclase fractionation trends (after Spulber and Rutherford, 1983; Sisson and Grove, 1993) the patterns of co-variation of major element oxides for the three chemical groups could be explained by crystal fractionation at different water pressures. The BGMV group is characterized by Al_2O_3 contents that remain relatively low even for the most evolved compositions and relatively higher TiO_2 abundances, which are more consistent with crystal fractionation under low-pressure dry condition (figs. 10A, B). In contrast, the BLMV and SMI groups are characterized by increasing Al contents in the range from basalt to basaltic andesite (fig. 10A). Some samples of these groups also display relatively low TiO_2 concentrations at similar SiO_2 content (fig. 10B). All these features are characteristics of calc-alkaline suite evolved through plagioclase fractionation at elevated water pressure. The interpretation is also supported by Cr versus MgO variation patterns (fig. 5I). In case of the BGMV samples Cr concentration decreases with increase in MgO wt%, implying fractionation under dry conditions where Cr behaves as an incompatible element in the absence of Fe-Ti oxide crystallization. A reverse situation, that is, increase of Cr abundance with MgO contents in the BLMV and SMI samples suggests early crystallization of Fe-Ti oxides under oxidizing wet conditions (O'Neil and others, 2011). It is also reflected in N-MORB normalized trace element diagrams, the BGMV group possesses insignificant Ti anomaly, which is large and negative in the BLMV and SMI groups (figs. 6D–F).

Petrogenesis of felsic rocks.— Petrogenetic types of the SGB felsic rocks.——The granitic rocks can be divided into I-, S- and A-types according to the nature of their source and petrogenesis (Chappell and White, 1992). In the $FeO_{total}/(FeO_{total} + MgO)$ versus SiO_2 diagram the SGB granites, quartz diorites and one sample of rhyolite fall in the magnesian I- to S-type granite field and the rest of the rhyolite samples, and agglomerate matrix and tuff samples fall in the ferroan A-type granite field (fig 11A).

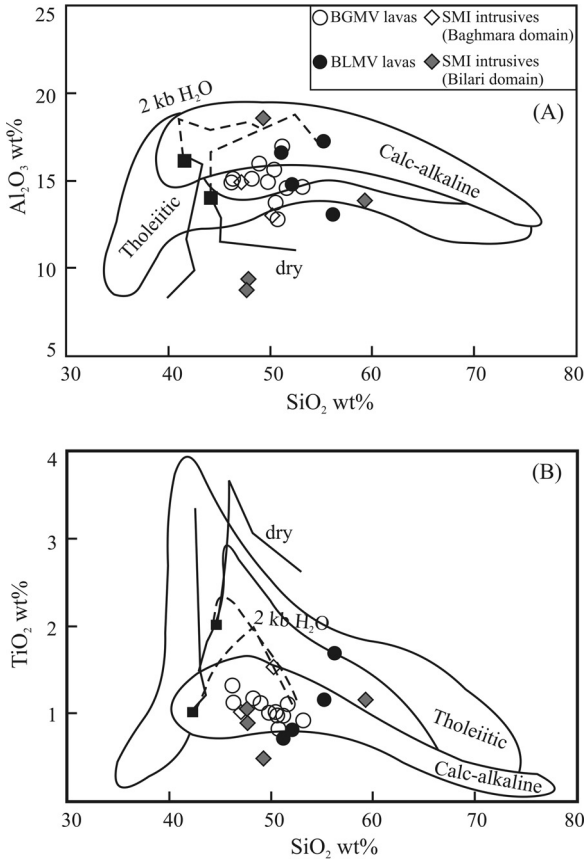

Fig. 10. Plots of Al_2O_3 versus SiO_2 (A) and TiO_2 versus SiO_2 (B) for SGB mafic rocks after Spulber and Rutherford (1983) and Sisson and Grove (1993), explaining conditions of fractionation of the parent magmas.

Moreover, the granites and quartz diorites have low concentrations of Zr+Nb+Ce+Y (less than or close to 350), $(K_2O+Na_2O)/CaO$ ratios (0.34–1.55) and values of $Ga/Al*10^3$ (1.80–2.55) and they fall in the undifferentiated field of I- and S-type granites (figs. 11B, C). It is noteworthy that these two rock types are strongly metaluminous, diopside-normative and contain amphibole. These features are considered to be important criteria for distinguishing I-type from S-type granitoids (Chappell and White, 1992). Therefore, the studied quartz diorites and granites are classified as I-type granite.

In contrast, rhyolites, ignimbrites, agglomerate matrix and tuff collectively have metaluminous to peralkaline transitional character and show high contents of total alkalis (3.66–8.99 wt%), HFSEs, REEs (except for Eu) and high values of Zr+Nb+Ce+Y (>350) and $Ga/Al*10^3$ (2.09–2.68), resembling in composition those of typical A-type granites worldwide (Eby, 1992; Johansson and others, 2016). They also plot in the A-type granite field in the various chemical classification diagrams (figs. 11B, C).

Petrogenesis.——Although the SGB felsic rock samples in majority belong to high-K calc-alkaline to alkaline series and are metaluminous and diopside normative, compositional variation, as addressed above, probably resulted from one or more of

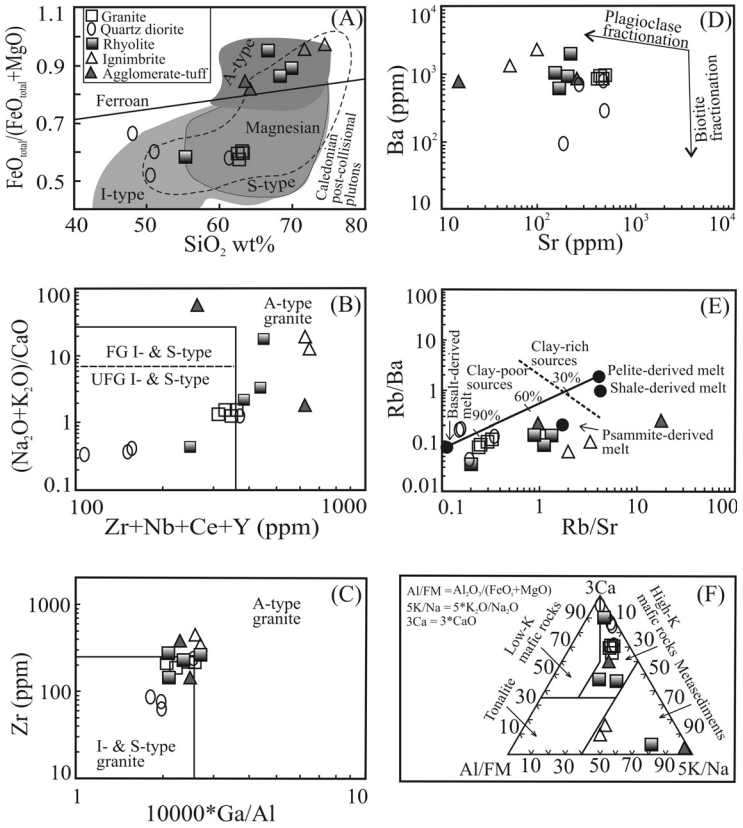

Fig. 11. (A) $FeO_{total}/(FeO_{total}+MgO)$ versus SiO_2 classification of SGB felsic rocks into I- S- and A-type granitoids after Frost and others (2001). (B, C) Plots of SGB felsic rocks in $(Na_2O+K_2O)/CaO$ versus (Zr+Nb+Ce+Y) and Zr versus 10000*Ga/Al discrimination diagrams after Whalen and others (1987). In (B) FG, fractionated granitic rocks; UFG, unfractionated granitic rocks. (D) Ba versus Sr variation revealing dominant plagioclase and biotite fractionation after Fowler and others (2008). (E), Rb/Ba versus Rb/Sr diagram revealing possible source of I- and A-type rocks of SGB. The mixing curve between basalt- and pelite-derived melts from Patino and others (1998) and Sylvester (1998). (F) CaO – Al_2O_3/$(FeO_{total}+MgO)$ – K_2O/Na_2O diagram after Laurent and others (2014), showing fields of source rocks of the SGB felsic rocks.

processes of fractional crystallization, magma mixing, crustal assimilation and partial melting. Quartz diorites and felsic volcanics show decrease of Al_2O_3, CaO, $Fe_2O_3{}^T$ and TiO_2 with increasing SiO_2 (Appendix fig. A1). Secondly, in chondrite and primitive mantle normalized diagrams, these rocks are characterized by weak to pronounced Eu and Sr anomalies (figs. 8A–D). Thus, fractionation of plagioclase, biotite, hornblende and K-feldspar during formation of these rocks is indicated. The Ba–Sr relationships provide information on feldspar and biotite fractionation (fig. 11D). More importantly, on the primitive mantle normalized multi-element diagrams (figs. 8C, D) all the felsic rocks of SGB, particularly the volcanic rock samples, show near-parallel patterns with relatively strong troughs at P and Ti. These patterns can be interpreted as the result of fractionation of apatite and Fe–Ti oxides (Eby, 1992, Fowler and others, 2008). However, the relatively low SiO_2 contents (<70 wt%), except ignimbrites, indicate that the fractionation process may not be a dominant mechanism. Although rare, apophyses of granite in metabasalts (fig. 3F) are indicative of the role

of magma mixing. On the other hand, the mafic microgranular enclaves, occasionally found in the granite and quartz diorite, stand for disruption of early biotite-enriched mushes due to batch melt (crustal) recharge in the magma chamber. Therefore, mixing of mantle derived melt with crustal one and recharge of parent melt by batch melt may have played some role in the petrogenesis of these rocks, though these are unlikely to have been major processes.

Compositional differences of the granitoid magmas produced by partial melting of different sources (for example ortho-amphibolites, metagreywackes, metapelites) under various melting conditions can be distinguished in terms of Rb/Ba and Rb/Sr ratios. In the Rb/Ba versus Rb/Sr diagram, the quartz diorite and granite samples plot close to the metabasaltic source melt (fig. 11E) and into the field for high-K mafic source in $CaO\text{-}Al_2O_3/(FeO_{total}+MgO)\text{-}K_2O/Na_2O$ diagram (fig. 11F). The parental melts of the felsic plutonic intrusives therefore originated from the mantle with or without recharge of crust-derived silicic batch melt. However, as addressed above, recharge of batch melt as well as magma mixing are not the main processes, responsible for petrogenesis in these rocks. It is remarkable that the depletion of Nb, Ta and Ti and enrichment of Zr and Hf, as displayed in primitive mantle-normalized trace element diagrams (figs. 8C, D) can be attributed to a mantle source for these rocks (Klemme and others, 2005). Moreover, besides calc-alkaline composition, these rocks are characterized by enrichment of LREEs and LILEs and depletion of HFSEs, implying an origin from lithospheric mantle that had been metasomatized by subduction-related processes (for example, Zhu and others, 2018). This interpretation is also supported by the Nb/La ratios of the studied rocks, which vary from 0.12 to 0.33. These ratios are consistent with a lithospheric mantle source (<0.5) but not an asthenospheric mantle source (ratio >1) because HFSEs like Nb and Ta are depleted in the lithospheric mantle relative to LILEs (Smith and others, 1999).

On the other hand, the rhyolites, ignimbrites, agglomerate matrix and tuff have higher Rb/Sr but lower Sr/Ba ratios. In the Rb/Ba versus Rb/Sr diagram, these rocks are dominantly clustered close to the clay-poor psammitic source, though, in $CaO\text{-}Al_2O_3/(FeO_{total}+MgO)\text{-}K_2O/Na_2O$ diagram they are distributed across the boundary between High-K mafic rocks and metasediments (figs. 11E, F). Thus, the processes involving dehydration-melting of biotite-bearing metagreywacke for the generation of parent magmas of the SGB felsic volcanic rocks is implied (Sylvester, 1998). However, as discussed above, the SGB felsic rocks have experienced a minor amount of crustal contamination. In summary, the parent magma of the felsic plutonic rocks of the SGB was possibly associated with the melting of enriched lithospheric mantle, whereas the volcanic rocks might have derived from partial melting of a metasediment-bearing source.

Tectonic Discrimination of the SGB Metaigneous Rocks

The Baghmara domain mafic volcanic rocks (BGMV group) represents a Low-K tholeiite suite, the parent magmas of which were possibly derived from a primitive mantle source with an N-MORB affinity. In contrast, the calc-alkaline suites of the Bilari domain mafic volcanic rocks (BLMV group) and the Sonakhan mafic intrusive rocks (SMI group) were originated from magmas, derived predominantly from partial melting of enriched mantle source at different depths, less and more deep for the BLMV and SMI groups, respectively. However, though the influence of weathering and metamorphism on the major element chemistry of mafic rocks is not unusual (Winchester and Floyd, 1976; Polat and others, 2003), the HFSE and HREE of mafic rocks are relatively immobile during mantle melting, low- to high-grade metamorphism, and moderate hydrothermal alteration (Pearce, 2008, 2014; Dilek and Furnes, 2009, 2011, 2014), and are thus helpful to discriminate possible tectonic settings of

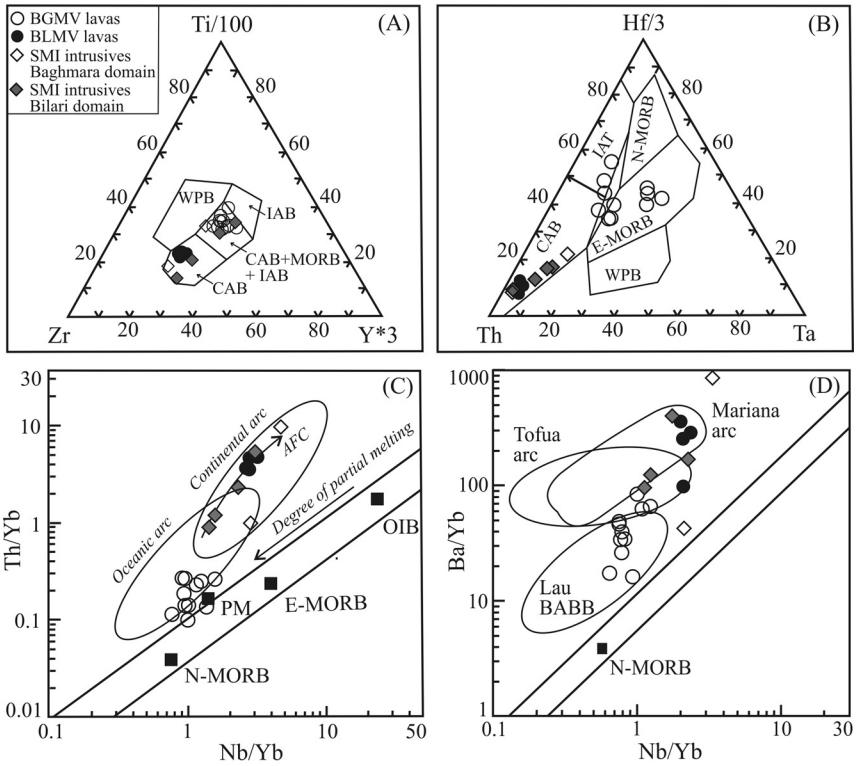

Fig. 12. Geochemical discrimination of the Sonakhan mafic rocks. (A) Ti-Zr-Y diagram after Pearce and Cann (1973). (B) Th-Hf/3-Ta diagram after Wood (1980). (C) Th/Yb versus Nb/Yb diagram, after Dilek and Furnes (2011) and Pearce (2014). PM – primitive mantle; MORB – mid-oceanic ridge basalt; E – enriched; N –normal; OIB – ocean island basalt. (D) Ba/Yb versus Nb/Yb diagram after Pearce and Stern (2006). BABB – back-arc basin basalt.

their magmatic evolution. Hence, on the basis of HFSE values, we have tested the status of the mafic volcanic and intrusive rocks of the SGB in different tectonic discrimination diagrams. In a Ti-Zr-Y diagram, all the BGMV and BLMV group samples plot in the field of ocean-floor basalts and calc-alkali basalts, respectively, whereas the SMI intrusive samples are distributed over these two fields (fig. 12A). However, when plotted in a Hf-Th-Ta diagram, the BGMV samples are clustered across the boundary between MORB and IAT fields, and all the BLMV and SMI rocks are restricted in the CAB field (fig. 12B). It is generally considered that contents of Th and Nb are significant to decipher the role of tectonic setting on mafic-ultramafic suites, and high values of Th/Yb ratio and of both Th/Yb and Nb/Yb ratios point to influence of subduction fluid-melt and of subduction together with AFC processes, respectively (Pearce, 2014). All the SGB mafic rock samples are plotted, in the Th/Yb versus Nb/Yb diagram, above the MORB-OIB mantle array. However, the BGMV samples are very close to this array and clustered around PM, whereas the plots of the BLMV and SMI rocks are distributed in the continental arc array, defining an AFC (assimilation and/or fractional crystallization) trend (fig. 12C), implying two distinct settings of extrusion of the BGMV group and the BLMV and SMI groups of rocks. Although in the V versus Ti diagram all the analyzed samples plot in MORB field, this inference is supported by the V/Ti ratios, which are close to 20 for the BGMV group and to 30 for both the BLMV and SMI groups (Appendix fig. A3). Similarly, it has been considered that the values of Ba/Nb

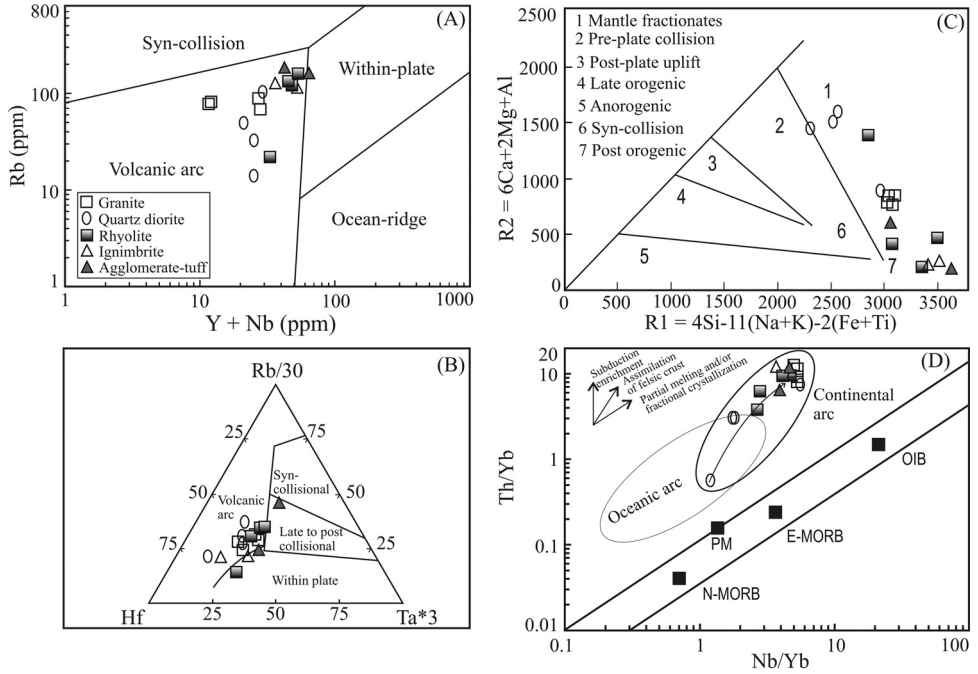

Fig. 13. Geochemical discrimination of the SGB felsic rocks. (A) Rb versus (Y+Nb) discrimination diagram after Pearce and others (1984). (B) Hf-Rb/30-Ta*3 discrimination diagram after Harris and others (1986). (C) R1-R2 diagram after De la Roche and others (1980). R1 = 4Si – 11(Na + K) – 2(Fe + Ti); R2 = (6Ca + 2Mg) + Al). (D) Th/Yb versus Nb/Yb tectonic discrimination diagram after Pearce (2008). Mixing lines after Mole and others (2021).

and Nb/Yb ratios are proxies to subduction input, a function of back-arc basin evolution, mantle flow patterns, and arc proximity, and of role of mantle flow around subduction edge, respectively. Hence, to evaluate the extent of subduction input in arc-basin system plotting Ba against Nb, using Yb as a normalizing factor to reduce the effects of fractional crystallization and crystal accumulation has been suggested (Pearce and Stern, 2006). In the Ba/Yb versus Nb/Yb diagram plots of all the SGB mafic rock samples define a broadly positive correlation, with the BGMV samples restricted in the field for Lau back-arc basin basalts and the BLMV and SMI samples straddled over those for Tofua arc and Mariana arc (fig. 12D). Thus, as displayed by the above data, the BLMV and SMI groups of rocks record the subduction influence, which in case of the BGMV parent magmas, if any, was possibly negligible. Recent studies suggest that during Neoarchean primitive mantle was geochemically enriched relative to N-MORB (for example, Mole and others, 2021). Therefore, although the BGMV samples have N-MORB type major element composition, their enriched Th concentrations are unlikely to be due to subduction, as these samples deviate along the mantle array (from N-MORB), rather than up into the arc-array for metasomatic source (fig. 12C).

On the other hand, though all the intermediate to acidic rock samples of the SGB plot in the field of volcanic arc in the Rb versus Y+Nb and Rb/30-Hf-Ta*3 discrimination diagrams (figs. 13A, B), the R_1–R_2 diagram confirms derivation of granites and quartz diorites as mantle melt fractionates and of rhyolite, ignimbrite, agglomerate and tuff as post orogenic extrusions (fig. 13C). Furthermore, the SGB felsic intrusives and volcanic rocks are potassic, low in Sr/Y ratio (fig. A 4), and in the

Th/Yb versus Nb/Yb diagram define a mixing trend between primitive mantle (PM) and continental crust (fig. 13D). However, formation of these felsic volcanic rocks in arc setting is also supported by the convex LILE abundance patterns in the primitive mantle normalized multi-element diagrams (figs. 8C, D).

Tectonic Model.—The Sonakhan greenstone belt (SGB) has close spatial association of sections of basaltic upper oceanic crust varying in geochemical signatures (MORB or Arc). However, the SGB lack any tectonized mantle section of ultramafic composition, or any palgiogranite. Though ophiolites may have diverse lithotectonic association and origin (Dilek and Furnes, 2011), the SGB is unlikely to represent an ophiolite suite. Rather this belt hosts two contrasting metaigneous suites, juxtaposed with each other, and the junction in-between is overlapped by the Arjuni Formation succession comparable to a Bouma sequence overlain by pelagic deposits. The mafic volcanic rocks dominated BGMV suite of the western SGB comprises multiple cycles of submarine eruption and sedimentation. The westernmost segment of the BGMV, with massive to pillowed basalt topped by chert-BIF-shale, represents relatively older, denser ridge-distal sequence, and it grades eastward into pillow breccia dominated ridge-proximal cycles with greywacke-shale at the top. The dominance of pillow breccia in the latter cycles indicates progressive eastward shallowing-up of the BGMV rift-ridge system. In contrast, geochemical data from the BLMV suite of the eastern SGB, outcropped immediately east of the Arjuni Formation succession, has distinct arc affinity. As discussed earlier, the BGMV-Arjuni Formation contact zone is represented by tectonic mélange as expected in accretionary wedges (Xiao and others, 2003; Pound and others, 2014). On the other hand, the granite and diorite stocks from both the domains host enclaves of metabasalt, metagreywacke and MME. Although the granite stocks of the Baghmara domain in the western part of the SGB are foliated, both the granite and diorite bodies of the Bilari domain in the eastern part of the SGB are essentially massive. Similarly, ignimbrite and rhyolite bodies, though, show interfingering or interbanded relations with metagreywacke or metabasalts, they are internally massive. Thus, the emplacement of these felsic plutonic and volcanic rocks possibly represents the waning phase of tectonic evolution of the belt.

We considered association of different rock units in the SGB, their deformation, geochemical characteristics of the metaigneous rocks, source characters, varied degrees of partial melting and magma fractionation under different water-pressure condition. Based on these and taking into account the regional geology of the Bastar craton including broadly contemporaneous supracrustals and granitoid plutons of the Dongargarh belt (Neogi and others, 1996; Narayana and others, 2000; Sensarma and Mukhopadhyay, 2014; Asthana and others, 2014), we propose the following tectonic evolutionary model (fig. 14).

In the northern part of the Bastar craton an oceanic realm possibly developed in the late Neoarchean, as evidenced by the extensive formation of supracrustals, dominated by bimodal volcanics and intercalated sediments in the Donargarh belt and its southern extension in the Kotri belt, dated about 2530 Ma (Neogi and others, 1996; Ghosh, 2004b). The Dongargarh batholith and similar other smaller granitic plutons, lying west of the unclassified granite gneisses (compare with Baya gneiss) and the SGB, are intrusive into relatively older supracrustals. Although heterogenous composition (I-type to A-type) of the Dongargarh batholith and post tectonic emplacement of the A-type granites of this batholith are interpreted (Narayana and others, 2000), we suggest that this plutonic complex is possibly a displaced remnant arc now lying west of the SGB. Initially the Bastar Neoarchean ocean possibly hosted an ancient arc (fig. 14A), which extended and rifted apart due to roll-back associated with a west vergent subduction system (fig. 14B). As discussed earlier, the N-MORB like geochemical affinity of the BGMV mafic volcanic rocks may as well represent segments of a back-arc

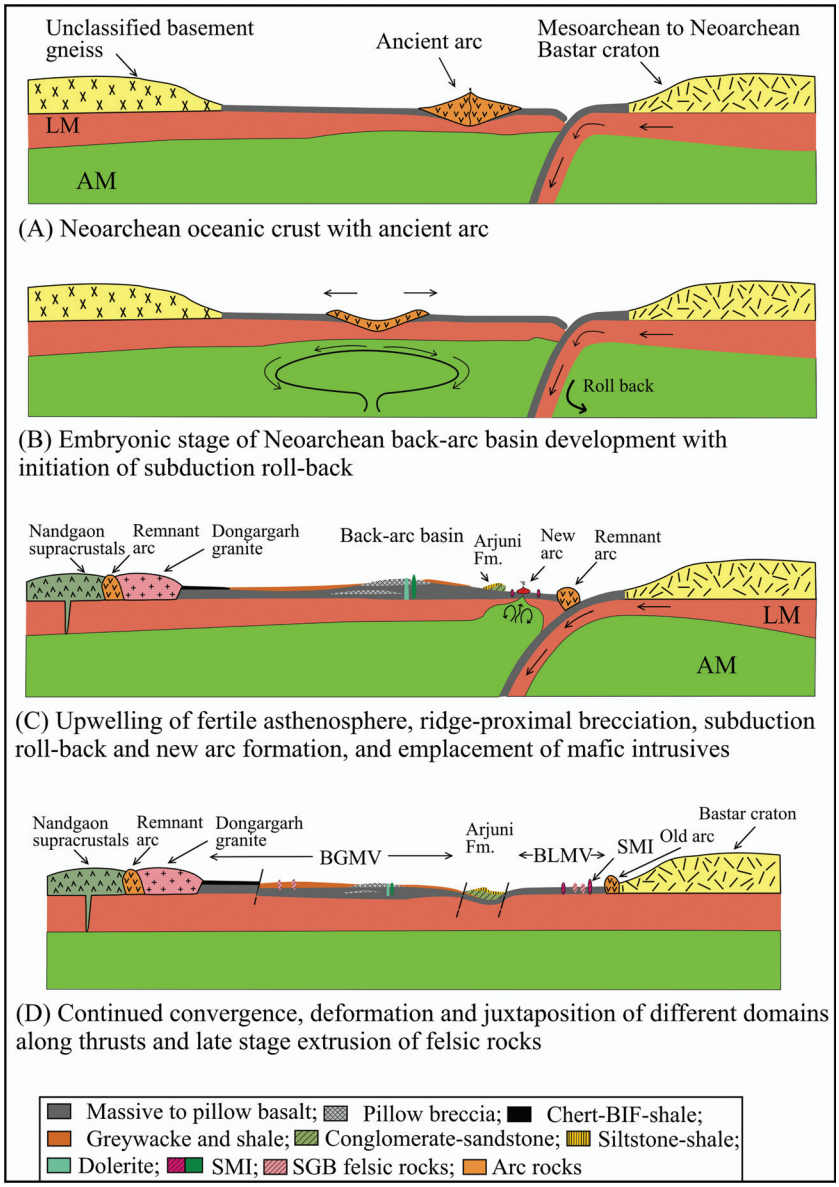

Fig. 14. Schematic diagram showing tectonic evolution of the Sonakhan greenstone belt. (A) Development of the Neoarchean Bastar ocean with an ancient arc above the subduction system. (B) Subduction roll-back and initiation of back-arc basin. (C) Development of matured back arc basin filled up by BGMV group overlain by deep to shallow marine sediments, and of magmatic arc (BLMV group), intrusion of SMI group and deposition of the Arjuni Formation. (D) Continued convergence, deformation, juxtaposition of different segments with MORB (BGMV, back-arc) and arc (BLMV and SMI) like geochemical signatures, and extrusion of felsic rocks. BGMV – Baghmara Mafic Volcanic group, BLMV – Bilari Mafic Volcanic group, SMI – Sonakhan Mafic Intrusives, LM – Lithospheric Mantle, AM – Asthenospheric Mantle.

basin which developed west of the volcanic arc formed above this intra-oceanic subduction system. The BLMV domain represents the eastern segment of the arc which was rifted and the back-arc basin opened up over a mantle upwelling as the west

vergent subducting slab continued to roll back (fig. 14C). The calc-alkaline magmas derived from enriched mantle source of spinel plus garnet lherzolitic composition, occurring in the BLMV of the Bilari domain in the eastern SGB, thus represent a segment of the intra-oceanic arc. Upwelling of fertile asthenosphere, decompression melting of spinel lhezolitic mantle and outpouring of the BGMV group lavas, now dominating in the Baghmara domain, represent initial back arc opening. Dolerite dike and intrusives of gabbro represent the probable axial zone of the back-arc ocean ridge system, while the rifted apart fragments of the ancient arc became part of the Dongargarh batholith in the west and of Bastar craton in the east (fig. 14C).

The back-arc basin filled up with multiple cycles of mainly mafic volcanic lavas and sediments, culminating in the development of polymictic conglomerate-greywacke-sandstone packets of the Arjuni Formation. Continued westward crustal convergence led to the deformation of the entire subduction complex and formation of relatively younger and less deformed intermediate to felsic calc-alkaline intrusions more extensive in the BLMV, but to a lesser extent also in the deformed BGMV (fig. 14D). This final stage was also accompanied with the emplacement of felsic extrusions derived through mixing of the upwelling asthenosphere induced partial melts, from subcrustal lithospheric mantle and/or metasedimentary source, and crustal materials.

CONCLUSION

Thrust-juxtaposed domains in the late Neoarchean – early Proterozoic Sonakhan greenstone belt (SGB), India has distinct volcano-sedimentary lithologic associations and the rock suites have geochemically distinct fingerprints. The Baghmara domain in the west is dominated by tholeiitic mafic volcanic rocks with N-MORB to primitive mantle character, similar to Parece Vela basin west of Mariana Arc. The Bilari domain in the east has preponderance of calc-alkaline mafic to felsic volcanic rocks suggesting arc like character. A polymictic conglomerate-greywacke succession lying in the middle and overlapping the other two units possibly represents back-arc basin fill over a basaltic substrate with common pillow basalts and pillow breccia reminiscent of a back-arc spreading centre. The sedimentary basin fill is partly derived from the rising arc and older basement.

Tectonic evolution of the SGB possibly followed early development of an intra-oceanic arc (remnant of which is in the Bilari domain), then subduction roll-back induced back-arc spreading and outpouring of the N-MORB like tholeiitic basalts of the Baghmara domain. Continued subduction and tectonic convergence led to folding and thrusting of these two domains as well as the back-arc basin fill sediments. The association of possible oceanic back-arc and arc segments in the late Neoarchean – early Proterozoic greenstone belts as in the SGB may be more common elsewhere, as modern style plate tectonic regime may have been operational by then.

ACKNOWLEDGMENTS

The study was supported by several grants from Indian Statistical Institute, Kolkata and FRPDF Scheme from Presidency University, Kolkata. Authors gratefully acknowledge the critical but constructive comments and suggestions from the journal reviewers, Prof. Yildirim Dilek and another anonymous reviewer, which helped immensely to improve the manuscript to its present state.

APPENDIX

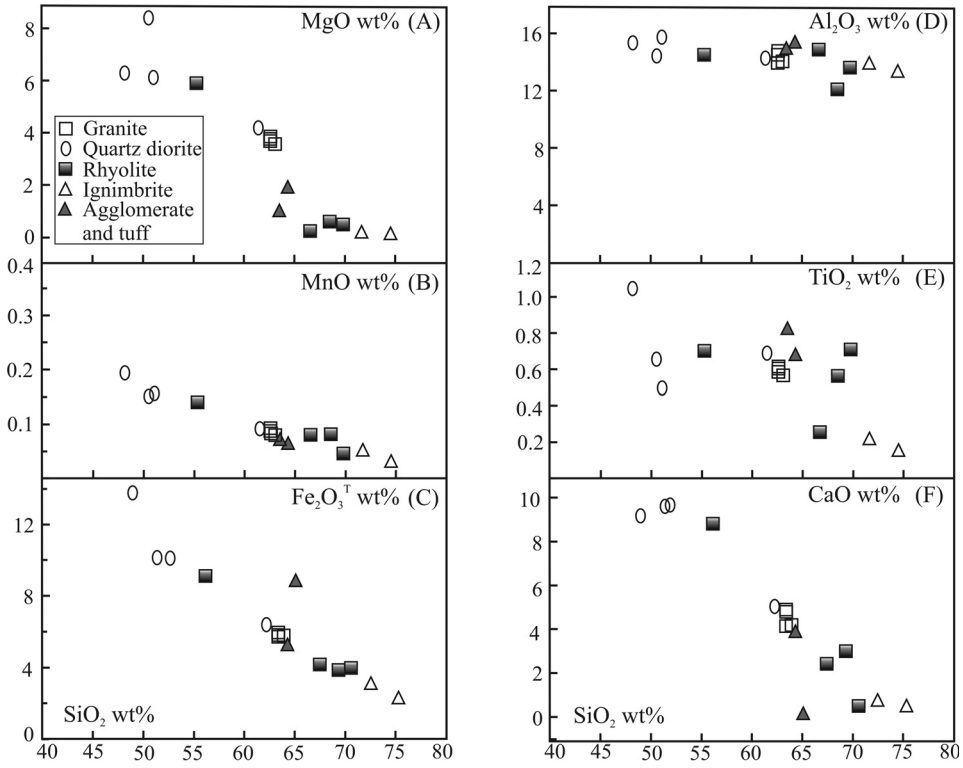

Fig. A1. Variation of selected major element oxides of Sonakhan felsic rocks against SiO_2, after Harker (1909).

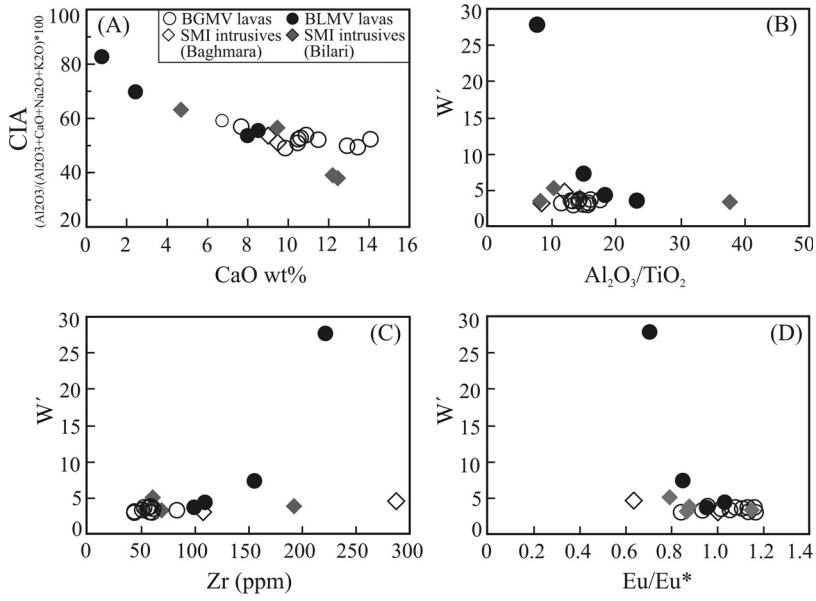

Fig. A2. Selected major and trace elements versus weathering Indices. (A), Negative correlation between CIA (after Nesbitt and Young, 1982) and CaO wt%. Weathering Index (W') values (after Ohta and Arai, 2007) of Sonakhan samples show persistently low W' and near constant Al_2O_3/TiO_2 (B), and no correlation with Zr (C) and Eu/Eu* (D).

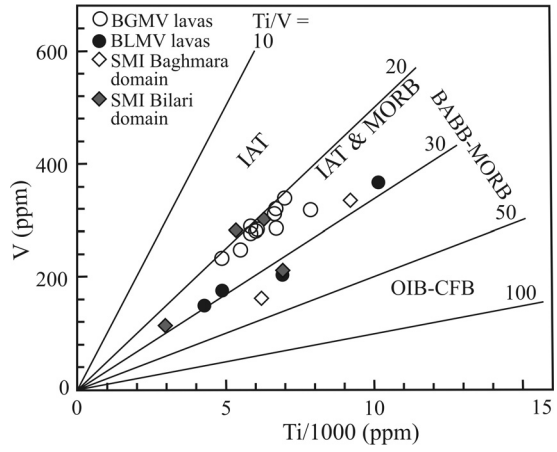

Fig. A3. Variation of SGB mafic rocks in Ti versus V diagram after Shervais (1982). IAT – island arc tholeiite; MORB – mid-oceanic ridge basalt; BABB – back-arc basin basalt; OIB – ocean island basalt; CFB – continental flood basalt.

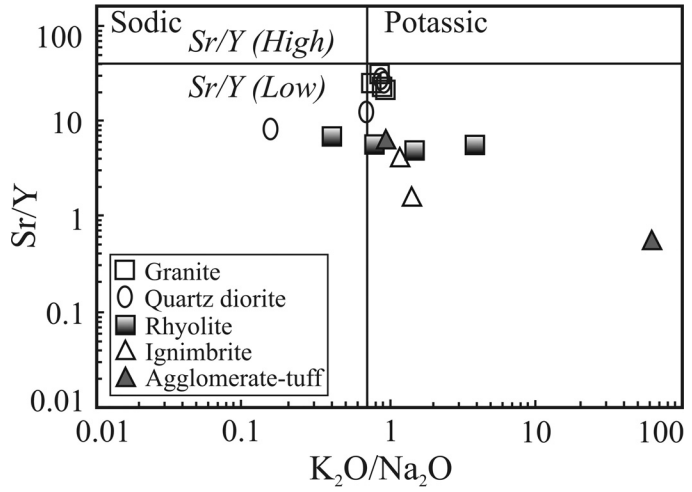

Fig. A4. Sr/Y versus K_2O/Na_2O diagram for discrimination of felsic-intermediate rocks; values for separation of areas from Moyen and Martin (2012) and Smithies and others (2018).

REFERENCES

Acharyya, S. K., and Roy, A., 2000, Tectonothermal history of the Central Indian Tectonic Zone and reactivation of major faults/shear zones: Journal Geological Society of India, v. 55, p. 239–256.

Ahmad, T., Wanjari, N., Kaulina, T. V., Mishra, M. K., and Nitkina, E. A., 2008, Geochemical and isotopic characteristics of the Amgaon gneissic complex, Central Indian Shield: Constraints on Precambrian crustal evolution, in Geoscience Resources and Environments of Asian Terranes (GREAT-2008): Proceedings International Symposium, 4th IGCP 516, and 5th APSEG, November 24–26, Bangkok, Thailand.

Aldanmaz, E., Pearce, J. A., Thirlwall, M. F., and Mitchell, J. G., 2000, Petrogenetic evolution of late Cenozoic, post-collision volcanism in western Anatolia, Turkey: Journal of Volcanology and Geothermal Research, v. 102, n. 1–2, p. 67–95, https://doi.org/10.1016/S0377-0273(00)00182-7

Asthana, D., Pophare, A. M., Rajalingam, S., and Kumar, H., 2014, Neoarchaean Dongargarh rapakivi A-type granites and its relationship to Pitepani tholeiites: Gondwana Geological Magazine, Special Volume 16, p. 25–40.

Barker, F., 1979, Trondhjemite: Definition, environment and hypothesis of origin, *in* Barker, F. editor, Trondhjemite, Dacite and Related Rocks: Elsevier, v. 6, p. 1–12, https://doi.org/10.1016/B978-0-444-41765-7.50006-X

Basu, A., and Bickford, M. E., 2015, An alternate perspective on the opening and closing of the intracratonic Purana basins in peninsular India: Journal of the Geological Society of India, v. 85, p. 5–25, https://doi.org/10.1007/s12594-015-0190-y

Bickford, M. E., Basu, A., Patranabis-Deb, S., Dhang, P. C., and Schieber, J., 2011, Depositional history of the Chhattisgarh basin, central India: constraints from new SHRIMP zircon ages: The Journal of Geology, v. 119, n. 1, p. 33–50, https://doi.org/10.1086/657300

Bickford, M. E., Basu, A., Kamenov, G. D., Mueller, P. A., Patranabis-Deb, S., and Mukherjee, A., 2014, Petrogenesis of 1000 Ma felsic tuffs, Chhattisgarh and Indravati basins, Bastar craton, India: Geochemical and Hf isotope constraints: The Joiurnal of Geology, v. 122, n.1, p. 43–54, https://doi.org/10.1086/674802

Bickle, M. J., and Teagle, D. A. H., 1992, Strontium alteration in the Troodos ophiolite: implication for fluid fluxes and geochemical transport in mid-ocean ridge hydrothermal systems: Earth and Planetary Science Letters, v. 113, n. 1–2, p. 219–237, https://doi.org/10.1016/0012-821X(92)90221-G

Blenkinsop, T. G., Fedo, C. M., Bickle, M. J., Eriksson, K. A., Martin, A., Nisbet, E.G., and Wilson, J. F., 1993, Ensialic origin for the Ngezi Group, Belingwe greenstone belt, Zimbabwe: Geology, v. 21, n. 12, p. 1135–1138, https://doi.org/10.1130/0091-7613(1993)021<1135:EOFTNG>2.3.CO;2

Bouma, A. H., 1962, Sedimentology of some Flysch deposits: A graphic approach to facies interpretation: Amsterdam, the Netherlands, Elsevier, 168 p.

Chappell, B. W., and White, A. J. R., 1992, I- and S-type granites in the Lachlan fold belt: Earth and Environmental Science Transactions of the Royal Society of Edinburgh, v. 83, n. 1–2, p. 1–26, https://doi.org/10.1017/S0263593300007720

Chavagnac, V., 2004, A geochemical and Nd isotopic study of Barberton komatiites (South Africa): implication for the Archean mantle: Lithos, v. 75, n. 3–4, p. 253–281, https://doi.org/10.1016/j.lithos.2004.03.001

Choudhary, A. K., Naik, A., Mukhopadhyay, D., and Gopalan, K., 1996, Rb-Sr dating of Sambalpur granodiorite, western Orissa: Journal Geological Society of India, v. 47, p. 503–506.
Condie, K. C., 1981, Archean Greenstone Belts: Amsterdam, the Netherlands, Elsevier, 433p.
Das, N., Royburman, K. J., Vatsa, U. S., Mahurkar, Y. V., and Dhoundial, D. P., 1990, Sonakhan Schist Belt, a Precambrian granite-greenstone complex: Geological Survey of India, Special Publication 28, p. 118–132.
Deb, G. K., 2013, Discussion of Saha et al. (2012, Precambrian Research) Tectono-magmatic evolution of the Mesoproterozoic Singhora basin, central India: Evidence for compressional tectonics from structural data, AMS study and geochemistry of basic rocks: Precambrian Research, v. 230, p. 248–257, https://doi.org/10.1016/j.precamres.2013.01.020
De la Roche, H., Leterrier, J., Grandclaude, P., and Marchal, M., 1980, A classification of volcanic and plutonic rocks using R_1-R_2 diagram and major-element analyses-its relationships with current nomenclature: Chemical Geology, v. 29, n. 1–4, p. 183–210, https://doi.org/10.1016/0009-2541(80)90020-0
de Wit, M. J., Armstrong, R. A., Hart, R. J., and Wilson, A. H., 1987, Felsic igneous rocks within the 3.3- to 3.5-Ga Barberton greenstone belt: High crustal level equivalents of surrounding Tonalite Trondhjemite Terrain, emplaced during thrusting: Tectonics, v. 6, n. 5, p. 529–549, https://doi.org/10.1029/TC006i005p00529
de Wit, M.J., and Ashwal, L.D., 1995, Greenstone belts: what are they?: South African Journal of Geology, v. 98, n. 4, p. 504–519, https://doi.org/10520/EJC-943d19ff8
Dilek, Y., and Furnes, H., 2009, Structure and geochemistry of Tethyan ophiolites and their petrogenesis in subduction rollback systems: Lithos, v. 113, n. 1–2, p. 1–20, https://doi.org/10.1016/j.lithos.2009.04.022
Dilek, Y., and Furnes, H., 2011, Ophiolite genesis and global tectonics: geochemical and tectonic fingerprinting of ancient oceanic lithosphere: Geological Society of America Bulletin, v. 123, n. 3–4, p. 387–411, https://doi.org/10.1130/B30446.1
Dilek, Y., and Furnes, H., 2014, Ophiolites and their origins: Elements, v. 10, n. 2, p. 93–100, https://doi.org/10.2113/gselements.10.2.93
Eby, G. N., 1992, Chemical subdivision of the A-type granitoids: petrogenetic and tectonic implications: Geology, v. 20, n. 7, p. 641–644, https://doi.org/10.1130/0091-7613(1992)020<0641:CSOTAT>2.3.CO;2
Fowler, M. B., Kocks, H., Darbyshire, D. P. F., and Greenwood, P. B., 2008, Petrogenesis of high Ba-Sr plutons from the Northern Highlands Terrane of the British Caledonian Province: Lithos, v. 105, n. 1–2, p. 129–148, https://doi.org/10.1016/j.lithos.2008.03.003
Frei, R., Rosing, M. T., Waight, T. E., and Ulfbeck, D. G., 2002, Hydrothermal-metasomatic and tectono-metamorphic processes in the Isua supracrustal belt (West Greenland): a multi-isotopic investigation of their effects on the earth's oldest oceanic crustal sequence: Geochimica et Cosmochimica Acta, v. 66, n. 3, p. 467–486, https://doi.org/10.1016/S0016-7037(01)00781-5
Frost, B. R., Barnes, C. G., Collins, W. J., Arculus, R. J., Ellis, D. J., and Frost, C.D., 2001, A geochemical classification for granitic rocks: Journal of Petrology, v. 42, n. 11, p. 2033–2048, https://doi.org/10.1093/petrology/42.11.2033
Ghosh, J. G., 2004a, 3.56 Ga tonalite in the central part of the Bastar craton, India: oldest Indian date: Journal of Asian Earth Science, v. 23, n. 3, p. 359–364, https://doi.org/10.1016/S1367-9120(03)00136-6
Ghosh, J. G., 2004b, Geochronological constraints of the evolution of the Kotri linear belt and its basement: Records Geological Survey of India, v. 137, n. 2, p. 24–26.
Ghosh, S., Rajajaiya, V., and Ashiya, I. D., 1995, Rb-Sr dating of components from the Sonakhan granite-greenstone belt, Raipur district, Madhyapradesh: Records Geological Survey of India, v. 128, p. 11–13.
Harker, A., 1909, The natural history of igneous rocks. New York, Macmillan, 384 p.
Harris, N. B. W., Pearce, J. A., and Tindle, A. G., 1986, Geochemical characteristics of collision zone magmatism, *in* Coward, M. P., and Reis, A. C., editors, Collision tectonics: Geological Society of London, Special Publication, v. 19, p. 67–81, https://doi.org/10.1144/GSL.SP.1986.019.01.04
Hart, S. R., 1971, K, Rb, Cs, Sr and Ba contents and Sr isotope ratios of ocean floor basalts: Philosophical Transaction of Royal Society London, Series A, Mathematical and Physical Sciences, v. 268, p. 573–87, https://doi.org/10.1098/rsta.1971.0013
Hastie, A. R., and Fitton, J. G., 2019, Eoarchaean tectonics: New constraints from high pressure-temperature experiments and mass balance modelling: Precambrian Research, v. 325, p. 20–38, https://doi.org/10.1016/j.precamres.2019.02.006
Hastie, A. R., Kerr, A. C., Pearce, J. A., and Mitchell, S. F., 2007, Classification of altered volcanic island arc rocks using immobile trace elements: development of the Th-Co discrimination diagram: Journal of Petrology, v. 48, n. 12, p. 2341–2357, https://doi.org/10.1093/petrology/egm062
Hawkins, J. W., 1976, Petrology and geochemistry of basaltic rocks of the Lau Basin: Earth and Planetary Science Letters, v. 28, n. 3, p. 283–297, https://doi.org/10.1016/0012-821X(76)90190-4
Hawkins, J. W., 1977, Petrologic and geochemical characteristics of marginal basin basalts, *in* Talwani, M., and Pitman, W. C., editors, Island Arcs, Deep Sea Trenches, and Back-Arc Basins, v. 1, p. 355–365, https://doi.org/10.1029/ME001p0355
Johansson, A., Waight, T., Andersen, T., and Simonsen, S. L., 2016, Geochemistry and petrogenesis of Mesoproterozoic A-type granitoids from the Danish island of Bornholm, southern Fennoscandia: Lithos, v. 244, p. 94–108, https://doi.org/10.1016/j.lithos.2015.11.031
Kelley, D. S., and Delaney, J. R., 1987, Two-phase separation and fracturing in mid-ocean ridge gabbros at temperature greater than 700 °C: Earth and Planetary Science Letters, v. 83, n. 1–4, p. 53–66, https://doi.org/10.1016/0012-821X(87)90050-1

Klemme, S., Prowatke, S., Hametner, K., and Günther, D., 2005, Partitioning of trace elements between rutile and silicate melts: implications for subduction zones: Geochimica et Cosmochimica Acta, v. 69, n.9, p. 2361–2371, https://doi.org/10.1016/j.gca.2004.11.015

Kröner, A., and Todt, W., 1988, Single zircon dating constraining the maximum age of the Barberton Greenstone Belt, southern Africa: Journal of Geophysical Research: Solid Earth, v. 93, n. B12, p. 15329–15337, https://doi.org/10.1029/JB093iB12p15329

Kusky, T. M., and Kidd, W. S. F., 1992, Remnants of an Archean oceanic plateau, Belingwe greenstone belt, Zimbabwe: Geology, v. 20, n. 1, p. 43–46, https://doi.org/10.1130/0091-7613(1992)020<0043:ROAAOP>2.3.CO;2

Laurent, O., Martin, H., Moyen, J. F., and Doucelance, R., 2014, The diversity and evolution of late-Archean granitoids: Evidence for the onset of "modern-style" plate tectonics between 3.0 and 2.5 Ga: Lithos, v. 205, p. 208–235, https://doi.org/10.1016/j.lithos.2014.06.012

Liu, F., Dilek, Y., Xie, Y., Yang, J., and Lian, D., 2018, Melt evolution of upper mantle peridotites and mafic dikes in the northern ophiolite belt of the western Yarlung Zangbo suture zone (southern Tibet): Lithosphere, v. 10, n. 1, p. 109–132, https://doi.org/10.1130/L689.1

Lowe, D. R., 1982, Sediment gravity flows: II. Depositional models with special reference to the deposits of high-density turbidity currents: Journal of Sedimentary Petrology, v. 52, n. 1, p. 279–297, https://doi.org/10.1306/212F7F31-2B24-11D7-8648000102C1865D

Maniar, P. D., and Piccoli, P. M., 1989, Tectonic discriminations of granitoids: Geological Society of America Bulletin, v. 101, n. 5, p. 635–643, https://doi.org/10.1130/0016-7606(1989)101<0635:TDOG>2.3.CO;2

Manu Prasanth, M. P., Hari, K. R., Chalapathi Rao, N. V., Hou, G., and Pandit, D., 2018, An island-arc tectonic setting for the Neoarchean Sonakhan Greenstone Belt, Bastar Craton, Central India: Insights from the chromite mineral chemistry and geochemistry of the siliceous high-Mg basalts (SHMB): Geological Journal, v. 53, n. 4, p. 1526–1542, https://doi.org/10.1002/gj.2971

Mattey, D. P., Marsh, N. G., and Tarney, J., 1980, The geochemistry, mineralogy and petrology of basalts from the West Philippine and Parece Vela Basins and from the Palau-Kyushu and West Mariana Ridges, Deep Sea Drilling Project Leg 59: Initial Report Deep Sea drilling Project 59, p. 753–800, https://doi.org/10.2973/dsdp.proc.59.137.1981

Mazumder, R., and Arima, M., 2009, Implication of mafic magmatism in an intracontinental rift setting: a case study from the Paleoproterozoic Dhanjori formation, Singhbhum crustal province, India: Journal of Geology, v. 117, n. 4, p. 455–466, https://doi.org/10.1086/599197

Miyashiro, A., 1974, Volcanic rock series in island arcs and active continental margins: American Journal of Science, v. 274, n. 4, p. 321–355, https://doi.org/10.2475/ajs.274.4.321

Mole, D. R., Thurston, P. C., Marsh, J. H., Stern, R. A., Ayer, J. A., Martin, L. A. J., and Lu, Y. J., 2021, The formation of Neoarchean continental crust in the south-east Superior Craton by two distinct geodynamic processes: Precambrian Research, v. 356. p. 106104, https://doi.org/10.1016/j.precamres.2021.106104

Mondal, M., and Raza, M., 2009, Tectonomagmatic evolution of the Bastar craton of Indian shield through plume-arc interaction, *in* Ahmad, T., Hirsch, F., and Charusiri, P., editors, Evidence from geochemistry of the mafic and felsic volcanic rocks of Sonakhan greenstone belt, Journal of the Virtual Explorer, v. 32, p. 3–22, https://doi.org/10.3809/jvirtex.2009.00245

Moyen, J.-F., and Martin, H., 2012, Forty years of TTG research: Lithos, v. 148, p. 312–336, https://doi.org/10.1016/j.lithos.2012.06.010

Narayana, B. L., Mallikharjuna Rao, J., Subba Rao, M. V., Murthy, N. N., and Divakara Rao, V., 2000, Geochemistry and Origin of Early Proterozoic Dongargarh Rapakivi Granite Complex, Central India - An Example for Magma Mixing and Differentiation: Gondwana Research, v. 3, n. 4, p. 507–520, https://doi.org/10.1016/S1342-937X(05)70757-7

Neogi, S., Miura, H., and Hariya, Y., 1996, Geochemistry of the Dongargarh volcanic rocks, Central India: Implications for the Precambrian mantle: Precambrian Research, v. 76, n. 1–2, p. 77–91, https://doi.org/10.1016/0301-9268(95)00025-9

Nesbitt, H. W., and Young, G. M., 1982, Early Proterozoic climates and plate motions inferred from major element chemistry of lutites: Nature, v. 299, p. 715–717, https://doi.org/10.1038/299715a0

O'Neil, J., Francis, D., and Carlson, R. W., 2011, Implications of the Nuvvuagittuq Greenstone Belt for the Formation of Earth's Early Crust: Journal of Petrology, v. 52, n. 5, p. 985–1009, https://doi.org/10.1093/petrology/egr014

Ohta, T., and Arai, H., 2007, Statistical empirical index of chemical weathering in igneous rocks: A new tool for evaluating the degree of weathering: Chemical Geology, v. 240, n. 3–4, p. 280–297, https://doi.org/10.1016/j.chemgeo.2007.02.017

Patiño Douce, A. E. P., and Harris, N., 1998, Experimental constraints on Himalayan anatexis: Journal of Petrology, v. 39, n. 4, p. 689–710, https://doi.org/10.1093/petroj/39.4.689

Patranabis-Deb, S., Bickford, M. E., Hill, B., Chaudhuri, A. K., and Basu, A., 2007, SHRIMF ages of zircon in the uppermost tuff in Chattisgarh Basin in central India require ~ 500 ma adjustment in Indian Proterozoic stratigraphy: Journal of Geology, v. 115, n. 4, p. 407–415, https://doi.org/10.1086/518049

Patranabis-Deb, S., and Chaudhuri, A.K., 2008, Sequence evolution in the eastern Chhattisgarh basin: constraints on correlation and stratigraphic analysis: The Palaeobotanist, v. 57, n. 1–2, p. 15–32.

Pearce, J. A., 2008, Geochemical fingerprinting of oceanic basalts with applications to ophiolite classification and the search for Archean oceanic crust: Lithos, v. 100, n. 1–4, p. 14–48, https://doi.org/10.1016/j.lithos.2007.06.016

Pearce, J. A., 2014, Immobile element fingerprinting of ophiolites: Elements, v. 10, n. 2, p. 101–108, https://doi.org/10.2113/gselements.10.2.101

Pearce, J. A., and Cann, J. R., 1973, Tectonic setting of basic volcanic rocks determined using trace element analyses: Earth and Planetary Science Letters, v. 19, n. 2, p. 290–300, https://doi.org/10.1016/0012-821X(73)90129-5

Pearce, J. A., and Stern, R. J., 2006, Origin of back-arc basin magmas: Trace element and isotope perspectives, *in* Christie, D. M., Fisher, C. R., Lee, S.-M., and Givens, S., editors, Back-arc spreading systems: Geological, biological, chemical and physical interactions: American Geophysical Union Geophysical Monograph, v.166, p. 63–86, https://doi.org/10.1029/166GM06

Pearce, J. A., Harris, N. B. W., and Tindle, A. G., 1984, Trace element discrimination diagrams for the tectonic interpretation of granitic rocks: Journal of Petrology, v. 25, n. 4, p. 956–983, https://doi.org/10.1093/petrology/25.4.956

Polat, A., and Hofmann, A. W., 2003, Alteration and geochemical patterns in the 3.7–3.8 Ga Isua greenstone belt, West Greenland: Precambrian Research, v. 126, n. 3–4, p. 197–218, https://doi.org/10.1016/S0301-9268(03)00095-0

Polat, A., and Kerrich, R., 2000, Archean greenstone belt magmatism and the continental growth-mantle evolution connection: Constraints from Th-U-Nb-LREE systematics of the 2.7 Ga Wawa Subprovince, Superior Province, Canada: Earth and Planetary Science Letters, v. 175, n. 1–2, p. 41–54, https://doi.org/10.1016/S0012-821X(99)00283-6

Polat, A., Regelous, M., Hofmann, A. W., and Appel, P. W. U., 2000, Contrasting geochemistry in the 3.7–3.8 Ga pillow basalt rims and cores, Isua greenstone belt, Greenland: implications for early Archean sea-floor alteration processes: EOS, Transactions, American Geophysical Union, v. 81, p. F1256.

Polat, A., Hofmann, A.W., and Rosing, M.T., 2002, Boninite-like volcanic rocks in the 3.7–3.8 Ga Isua greenstone belt, West Greenland: Geochemical evidence for intra-oceanic subduction zone processes in the early Earth: Chemical Geology, v. 184, n. 3–4, p. 231–254, https://doi.org/10.1016/S0009-2541(01)00363-1

Polat, A., Hofmann, A. W., Munker, C., Regelous, M., and Appel, P. W. U., 2003, Contrasting geochemical patterns in the 3.7–3.8 Ga pillow basalt cores and rims, Isua greenstone belt, Southwest Greenland: implications for post-magmatic alteration processes: Geochimica et Cosmochimica Acta, v. 67, n. 3, p. 441–457, https://doi.org/10.1016/S0016-7037(02)01094-3

Polat, A., Wang, L., and Appel, P. W. U., 2015, A review of structural patterns and melting processes in the Archean craton of West Greenland: Evidence for crustal growth at convergent plate margins as opposed to non-uniformitarian models: Tectonophysics, v. 662, p. 67–94, https://doi.org/10.1016/j.tecto.2015.04.006

Pound, K. S., Norris, R. J., and Landis, C. A., 2014, Eyre Creek Mélange and accretionary prism shear-zone mélange in Caples Terrane rocks, Eyre Creek, northern Southland, New Zealand: New Zealand Journal of Geology and Geophysics, v. 57, n. 1, p. 1–20, https://doi.org/10.1080/00288306.2013.837395

Rollinson, H. R., 2007, Early Earth Systems, a geochemical approach: Oxford, United Kingdom, Blackwell Publishing, 285 p.

Roy, A., Prasad, M. H., and Bhowmik, S. K., 2001, Recognition of pre-Grenvillian and Grenvillian tectonothermal events in the Central Indian Tectonic Zones: Implications on Rodinian crustal assembly: Gondwana Research, v. 4, n. 4, p. 755–757, https://doi.org/10.1016/S1342-937X(05)70548-7

Saha, D., Deb, G. K., and Dutta, S., 2004, Granite-greenstone relationship in the Sonakhan Belt, Raipur District, central India: Geological Survey of India Special Publication Series, v. 57, p. 67–78.

Saha, D., Mazumder, R., and Kar, R., 2017, Shallow marine to pelagic sediments from a dismembered ophiolite, Kandra, southern India- Glimpses of ancient subduction zone related sedimentation: Gondwana Research, v. 49, p. 21–41, https://doi.org/10.1016/j.gr.2017.04.032

Saha, D., Bachhar, P., Deb, G. K., Patranabis Deb, S., and Banerjee, A., 2021, Tectonic evolution of the Paleoarchean to Mesoarchean Badampahar-Gorumahisani belt, Singhbhum craton, India - Implications for coexisting arc and plume signatures in a granite-greenstone terrain: Precambrian Research, v. 357, p. 106094, https://doi.org/10.1016/j.precamres.2021.106094

Sain, A., and Saha, D., 2018, Structure and tectonics of a Mesoproterozoic ophiolite - insight from Kanigiri Ophiolite with mélange zone, southern India: Tectonophysics, v. 744, p. 177–204, https://doi.org/10.1016/j.tecto.2018.06.017

Sarkar, A., Sarkar, G., Paul, D. K., and Mitra, N. D., 1990, Precambrian geochronology of the central Indian shield: a review: Geological Survey of India Special Publication, v. 28, p. 453–482.

Saunders, A. D., and Tarney, J., 1979, The geochemistry of basalts from a back-arc spreading centre in the East Scotia Sea: Geochimica Cosmochimica Acta, v. 43, n. 4, p. 555–572, https://doi.org/10.1016/0016-7037(79)90165-0

Saunders, A. D., and Tarney, J., 1984, Geochemical characteristics of basaltic volcanism within back-arc basins: Geological Society London, Special Publications, v. 16, p. 59–76, https://doi.org/10.1144/GSL.SP.1984.016.01.05

Sensarma, S., and Mukhopadhyay, D., 2014, Stratigraphy of ~2.5 Ga Dongargarh Belt, Central India: Key Observations and Suggested Revisions: Gondwana Geological Magazine, Special Volume 16, p. 41–48.

Shervais, J. W., 1982, Ti-V plots and the petrogenesis of modern and ophiolitic lavas: Earth and Planetary Science Letters, v. 59, n. 1, p. 110–118, https://doi.org/10.1016/0012-821X(82)90120-0

Shervais, J. W., 2001, Birth, death and resurrection: the life cycle of suprasubduction zone ophiolites: Geochemistry, Geophysics, Geosystems, v. 2, n. 1, p. 2000GC000080, https://doi.org/10.1029/2000GC000080

Shervais, J. W., Reagan, M., Haugen, E., Almeev, R. R., Pearce, J. A., Prytulak, J., Ryan, J. G., Whattam, S. A., Godard, M., Chapman, T., Li, H., Kurz, W., Nelson, W. R., Heaton, D., Kirchenbaur, M., Shimizu, K., Sakuyama, T., Li, Y., and Vetter, S. K., 2019, Magmatic Response to Subduction Initiation: Part 1. Fore-

arc Basalts of the Izu-Bonin Arc From IODP Expedition 352: Geochemistry, Geophysics, Geosystems, v. 20, n. 1, p. 314–338, https://doi.org/10.1029/2018GC007731
Singh, Y., and Chabria, T., 2002, Early Proterozoic 87Rb/86Sr model ages of pegmatitic muscovite from rare metal-bearing granite-pegmatite system of Kawadgaon, Bastar craton, central India: Gondwana Research, v. 5, n. 4, p. 889–893, https://doi.org/10.1016/S1342-937X(05)70924-2
Sisson, T. W., and Grove, T. L., 1993, Experimental investigations of the role of H2O in calc-alkaline differentiation and subduction zone magmatism: Contributions to Mineralogy and Petrology, v. 113, p. 143–166, https://doi.org/10.1007/BF00283225
Smith, E. I., Sánchez, A., Walker, J. D., and Wang, K., 1999, Geochemistry of mafic magmas in the hurricane Volcanic Field, Utah: implications for small- and large-scale chemical variability of the lithospheric mantle: Journal of Geology, v. 107, v. 4, p. 433–448, https://doi.org/10.1086/314355
Smithies, R. H., Champion, D. C., and Sun, S.-S, 2004, The case for Archean boninites: Contributions to Mineralogy and Petrology, v. 147, p. 705–721, https://doi.org/10.1007/s00410-004-0579-x
Smithies, R. H., Lu, Y., Gessner, K., Wingate, M. T. D., and Champion, D. C., 2018, Geochemistry of Archean granitic rocks in the South West Terrane of the Yilgarn Craton: Geological Survey of Western Australia, Record 2018/10.
Sotiriou, P., Polat, A., Frei, R., Yang, X.-M., and van Vessem, J., 2020, Evidence for Neoarchean hydrous arc magmatism, the anorthosite-bearing Mayville Intrusion, western Superior Province, Canada: Lithos, v. 362–363, p. 105482, https://doi.org/10.1016/j.lithos.2020.105482
Spulber, S. D., and Rutherford, M. J., 1983, The origin of rhyolite and plagiogranite in oceanic crust: an experimental study: Journal of Petrology, v. 24, n. 1, p. 1–25, https://doi.org/10.1093/petrology/24.1.1
Srivastava, R. K., and Gautam, G. C., 2008, Precambrian mafic dyke swarms from the southern Bastar, central India craton: present and future perspectives, *in* Srivastava, R. K., Srivastava, C. S., and Chalapatthi Rao, N. V., editors, Indian Dykes, Geochemistry, Geophysics and Geochronology: New Delhi, India, Narosa Publishing house Pvt. Ltd., p. 367–376.
Stern, R. J., 2008, Modern-style plate tectonics began in Neoproterozoic time: An alternative interpretation of Earth's tectonic history, *in* Condie, K. C., and Pease, V., editors, When Did Plate Tectonics Begin on Planet Earth?: Geological Society of America Special Paper, v. 440, p. 265–279, https://doi.org/10.1130/2008.2440(13)
Sun, S. S., and McDonough, W. F., 1989, Chemical and isotopic systematic of oceanic basalts: implications for mantle composition and processes, *in* Saunders, A. D., and Norry, M. J., editors, Magmatism in the oceanic basins: Geological Society of London, Special Publication, v. 42, p. 313–345, https://doi.org/10.1144/GSL.SP.1989.042.01.19
Sylvester, P. J., 1998, Post-collisional strongly peraluminous granites: Lithos, v. 45, n. 1–4, p. 29–44, https://doi.org/10.1016/S0024-4937(98)00024-3
Wakabayashi, J., 2017, Structural context and variation of ocean plate stratigraphy, Franciscan Complex of California: Insight into mélange origins and subduction -accretion processes: Progress in Earth and Planetary Sciences, v. 4, n. 18, p. 1–23, https://doi.org/10.1186/s40645-017-0132-y
Walker, R. G., 1978, Deep-water sandstone facies and ancient submarine fans: model for exploration for stratigraphic traps: American Association of Petroleum Geologists Bulletin, v. 62, n. 6, p. 932–966, https://doi.org/10.1306/C1EA4F77-16C9-11D7-8645000102C1865D
Whalen, J. B., Currie, K. L., and Chappell, B. W., 1987, A-type granites: geochemical characteristics, discrimination and petrogenesis: Contributions to Mineralogy and Petrology, v. 95, p. 407–419, https://doi.org/10.1007/BF00402202
Whattam, S. A., and Stern, R. J., 2011, The 'subduction initiation rule': a key for linking ophiolites, intra-oceanic forearcs, and subduction initiation: Contributions to Mineralogy and Petrology, v. 162, p. 1031–1045, https://doi.org/10.1007/s00410-011-0638-z
Wilkinson, J. F. G., 1982, The genesis of mid-ocean ridge basalt: Earth-Science Reviews, v. 18, n. 1, p. 1–57, https://doi.org/10.1016/0012-8252(82)90002-2
Wilson, M., 1989, Igneous Petrogenesis: A Global Tectonic Approach: Dordrecht, the Netherlands, Springer, 466 p, https://doi.org/10.1007/978-1-4020-6788-4
Winchester, J. A., and Floyd, P. A., 1976, Geochemical magma type discrimination, application to altered and metamorphosed basic igneous rocks: Earth and Planetary Science Letters, v. 28, n. 3, p. 459–469, https://doi.org/10.1016/0012-821X(76)90207-7
Winchester, J. A., and Floyd, P. A., 1977, Geochemical discrimination of different magma series and their differentiation products using immobile elements: Chemical Geology, v. 20, p. 325–343, https://doi.org/10.1016/0009-2541(77)90057-2
Windley, B. F., Kusky, T., and Polat, A., 2021, Onset of Plate Tectonics by the Eoarchean: Precambrian Research, v. 352, p. 105980, https://doi.org/10.1016/j.precamres.2020.105980
Wood, D. A., 1980, The application of a Th-Hf-Ta diagram to problems of tectonomagmatic classification and to establishing the nature of crustal contamination of basaltic lavas of the British tertiary Volcanic Province: Earth and Planetary Science Letters, v. 50, n. 1, p. 11–30, https://doi.org/10.1016/0012-821X(80)90116-8
Wood, D. A., Marsh, N. G., Tarney, J., Joron, J.-L., Fryer, P., and Treuil, M., 1981, Geochemistry of igneous rocks recovered from a transect across the Mariana Trough, Arc, Fore-arc, and Trench, Sites 453 through 461, Deep Sea Drilling Project Leg 60, Initial Report Deep Sea drilling Project 60, p. 611–645, https://doi.org/10.2973/dsdp.proc.60.133.1982
Workman, R. K., and Hart, S. R., 2005, Major and trace element composition of the depleted MORB mantle (DMM): Earth and Planetary Science Letters, v. 231, n. 1–2, p. 53–72, https://doi.org/10.1016/j.epsl.2004.12.005

Xiao, W., Windley, B. F., Hao, J., and Zhai, M., 2003, Accretion leading to collision and the Permian Solonker suture, Inner Mongolia, China: Termination of the central Asian orogenic belt: Tectonics, v. 22, n. 6, p. 8–20, https://doi.org/10.1029/2002TC001484

Zhu, J., Li, Q., Chen, X., Tang, H., Wang, Z., Chen, Y., Liu, S., Xiao, B., and Chen, J., 2018, Geochemistry and petrogenesis of the early Paleozoic appinite-granite complex in the Western Kunlun Orogenic Belt, NW China: implications for Paleozoic tectonic evolution: Geological Magazine, v. 155, n. 8, p. 1641–1666, https://doi.org/10.1017/S0016756817000450